

Adaptive Sampling-Based Bi-Fidelity Stochastic Trust Region Method for Derivative-Free Stochastic Optimization

Yunsoo Ha^{*1} and Juliane Mueller^{†1}

¹Computational Science Center, National Renewable Energy Laboratory,
15013 Denver West Parkway, Golden, 80401, Colorado, USA

Abstract

Bi-fidelity stochastic optimization has gained increasing attention as an efficient approach to reduce computational costs by leveraging a *low-fidelity* (LF) model to optimize an expensive *high-fidelity* (HF) objective. In this paper, we propose ASTRO-BFDF, an adaptive sampling trust region method specifically designed for unconstrained bi-fidelity stochastic derivative-free optimization problems. In ASTRO-BFDF, the LF function serves two purposes: (i) to identify better iterates for the HF function when the optimization process indicates a high correlation between them, and (ii) to reduce the variance of the HF function estimates using bi-fidelity Monte Carlo (BFMC). The algorithm dynamically determines sample sizes while adaptively choosing between crude Monte Carlo and BFMC to balance the trade-off between optimization and sampling errors. We prove that the iterates generated by ASTRO-BFDF converge to the first-order stationary point almost surely. Additionally, we demonstrate the effectiveness of the proposed algorithm through numerical experiments on synthetic problems and simulation optimization problems involving discrete event systems.

1 Introduction

We consider the stochastic optimization (SO) problem

$$\min_{\mathbf{x} \in \Re^d} f^h(\mathbf{x}) = \mathbb{E}_{\Xi^h}[F^h(\mathbf{x}, \xi^h)], \quad (1)$$

where $f^h : \Re^d \rightarrow \Re$ is nonconvex and bounded from below, $F^h : \Re^d \times \Xi^h \rightarrow \Re$ is a random function, and $\xi^h : \Omega \rightarrow \Xi^h$ is a random element. In particular, we are interested in the case where $f^h(\mathbf{x})$ can only be observed with noise through evaluations of $F^h(\mathbf{x}, \xi^h)$. Consequently, an estimator of $f^h(\mathbf{x})$ is obtained by repeatedly evaluating F^h , as shown below:

$$\bar{F}^h(\mathbf{x}, n) = \frac{1}{n} \sum_{i=1}^n F^h(\mathbf{x}, \xi_i^h), \quad (2)$$

and an estimate of the variance is computed as

$$(\hat{\sigma}^h)^2(\mathbf{x}, n) = n^{-1} \sum_{i=1}^n \left(F^h(\mathbf{x}, \xi_i^h) - \bar{F}^h(\mathbf{x}, n) \right)^2.$$

^{*}yunsoo.ha@nrel.gov

[†]juliane.mueller@nrel.gov

Furthermore, we assume that derivative information is not directly available from a Monte Carlo simulation, and each evaluation of F^h is computationally expensive. Consequently, the main challenge in solving Problem (1) lies in the need for a large number of model evaluations. One way to mitigate this burden is through bi-fidelity techniques, which leverage both a high-fidelity (HF) model and a low-fidelity (LF) model that is computationally cheaper but less accurate. For example, the LF model primarily helps identify promising solution candidates, while the HF model is used to further evaluate and refine those candidates. Hence, we assume that there exists an additional stochastic simulation oracle capable of approximating $F^h(\mathbf{x}, \xi^h)$ at a lower cost. This cost-effective oracle, termed the LF simulation, generates $F^\ell : \Re^d \times \Xi^\ell \rightarrow \Re$ with $f^\ell(\mathbf{x}) = \mathbb{E}_{\Xi^\ell}[F^\ell(\mathbf{x}, \xi^\ell)]$, where $\xi^\ell : \Omega \rightarrow \Xi^\ell$ is a random element. This framework is commonly referred to as *bi-fidelity stochastic optimization* (BFSO) and has recently gained popularity due to advancements in digital twins, with applications in manufacturing [1], production [2, 3], and engineering design [4, 5, 6].

HF and LF stochastic simulation models are typically developed through hierarchical modeling, where the HF model captures all relevant system details, while the LF model provides a simplified approximation. For example, in manufacturing systems, the HF model simulates a complete process including all machines, whereas the LF model is obtained by excluding machines that are not critical to the performance metrics (see Figure 8 in [3]). In airfoil design, fidelity is controlled by mesh resolution: the HF model uses a fine grid with many nodes around the airfoil, whereas LF models are generated by coarsening the mesh, thereby reducing computational cost (see Figure 17 in [7]). In discrete event simulation (DES), fidelity levels can be adjusted by changing simulation run length; the HF model uses long simulation runs to obtain accurate estimates, whereas LF models use shorter runs for faster evaluation [8].

Multi-fidelity approaches have primarily been used in Bayesian optimization (BO) with Co-kriging serving as the surrogate model due to its flexibility [9]. Most of the existing literature focuses on deterministic engineering design problems [10, 11, 12, 13, 14], since BO tends to perform poorly in the presence of high stochastic noise [15, 16, 17]. Specifically, the sample size n must be sufficiently large to ensure accurate function estimates, which becomes especially challenging when dealing with heteroskedastic variances [18]. Moreover, the LF function should remain closely correlated with the HF function throughout the entire search space, as BO is a global optimization method [19]. Otherwise, the LF function can negatively impact the surrogate model, reducing its accuracy [20, 21]. For instance, the LF function may provide no useful information about the HF function, which disrupts the optimization process, as illustrated in Figure 1. Hence, the specifics of how and when to utilize the LF simulation oracle have remained elusive, prompting us to pose two overarching questions:

- Q1. When is it appropriate to utilize the LF simulation oracle, and when should it not be used during optimization?
- Q2. What sample sizes for HF and LF simulation oracles are necessary to attain sufficiently accurate function estimates for optimization?

In this paper, we propose a *sample-efficient* local search solver for BFSO, aiming to address questions Q1 and Q2. We begin by introducing relevant existing sampling methods that have been used for sample-efficient uncertainty quantification, regardless of their purpose for optimization.

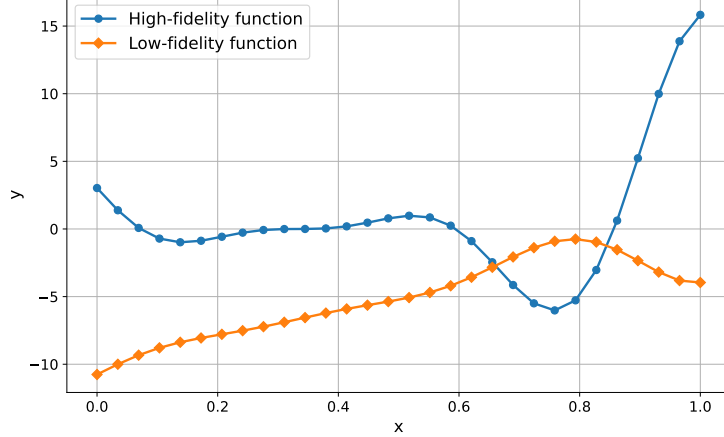


FIGURE 1: An illustration of bi-fidelity functions, where the LF function serves as a harmful source.

1.1 Adaptive Sampling

In derivative-free stochastic optimization, a suitable sample size is essential for reducing computational cost while ensuring the convergence of the solution sequence $\{\mathbf{X}_k\}$ to a stationary point. Typically, when the random samples $\{\xi_i^h\}_{i=1}^n$ vary across evaluations of x , a fixed sample size may fail to ensure almost sure convergence because the stochastic error may exceed the gap in function values between successive iterates. Therefore, an Adaptive Sampling (AS) strategy has been incorporated into iterative algorithms [22, 23, 24]. The AS strategy dynamically determines the sample size by balancing an estimation error at each point against an optimality measure such as gradient approximations. With the estimation error continuously updated through replicated function evaluations, the AS strategy selects a dynamically adjusted sample size based on observations generated at the design point of interest. The AS strategy has been proposed using a crude Monte Carlo (CMC) estimation (See (2)) for scenarios where only one simulation oracle is available [22, 24, 25]. However, when multiple simulation oracles of different fidelities are available, a variance reduction technique known as multi-fidelity Monte Carlo (MFMC) [26] can be employed, as introduced in the next section.

1.2 Bi-fidelity Monte Carlo

In the domain of uncertainty quantification, a function estimate for a single design point is typically derived through a CMC estimation. However, due to the slow convergence rate of CMC, where the estimation error decays at a rate proportional to $1/\sqrt{n}$, it may be impractical to obtain sufficiently accurate function estimates within a reasonable timeframe. To improve computational efficiency, bi-fidelity Monte Carlo (BFMC) has been proposed as a variance reduction methods [26], with the unbiased estimator defined as:

$$\bar{F}^{\text{bf}}(\mathbf{x}, n, v, c) = \frac{1}{n} \sum_{i=1}^n F^h(\mathbf{x}, \xi_i^h) - c \left(\frac{1}{n} \sum_{j=1}^n F^\ell(\mathbf{x}, \xi_j^\ell) - \frac{1}{v} \sum_{j=1}^v F^\ell(\mathbf{x}, \xi_j^\ell) \right), \quad (3)$$

where v is the sample size for the LF oracle and $c \in \Re$. The variance of $\bar{F}^{\text{bf}}(\mathbf{x}, n, v, c)$ is

$$\begin{aligned} & c^2(\text{Var}(\bar{F}^l(\mathbf{x}, n)) + \text{Var}(\bar{F}^l(\mathbf{x}, v))) - 2c\text{Cov}(\bar{F}^h(\mathbf{x}, n), \bar{F}^l(\mathbf{x}, n)) \\ & + 2c\text{Cov}(\bar{F}^h(\mathbf{x}, n), \bar{F}^l(\mathbf{x}, v)) - 2c^2\text{Cov}(\bar{F}^l(\mathbf{x}, n), \bar{F}^l(\mathbf{x}, v)) + \text{Var}(\bar{F}^h(\mathbf{x}, n)). \end{aligned} \quad (4)$$

Therefore, variance reduction becomes feasible when strong correlation exists between HF and LF estimators and appropriate values of n, v , and c are chosen. The effectiveness of such variance reduction has been empirically demonstrated in [27, 28].

In our proposed algorithm, we have developed an innovative AS strategy, referred to as bi-fidelity Adaptive Sampling (BFAS), that leverages both LF and HF oracles. Our approach dynamically employs BFMC and CMC, guided by covariance and variance estimates for the functions. Although BFAS can, in principle, be applied to a broad range of iterative solvers, we focus exclusively on stochastic trust region (TR) algorithms for solving Problem (1).

1.3 Stochastic Trust Region Algorithms for Derivative-free Stochastic Optimization

The popularity of stochastic TR algorithms has recently surged for addressing (1) due to their robustness, which comes from their ability to self-tune and naturally utilize approximate curvature information in determining step lengths. Stochastic TR algorithms [29, 30, 31, 32] typically involve the following four steps in each iteration k :

- (a) (model construction) a local model is constructed to approximate the objective function f by utilizing specific design points and their function estimates within a designated area of confidence, i.e., the TR, typically defined as an ℓ_2 ball with radius Δ_k centered at the current iterate \mathbf{X}_k ;
- (b) (subproblem minimization) a candidate point \mathbf{X}_k^s is obtained by approximately minimizing the local model within the TR;
- (c) (candidate evaluation) the objective function at \mathbf{X}_k^s is estimated by querying the oracle, and depending on this evaluation, \mathbf{X}_k^s is either accepted or rejected; and
- (d) (TR management) if \mathbf{X}_k^s is accepted, it becomes the next iterate \mathbf{X}_{k+1} , and the TR radius Δ_k is either enlarged or remains unchanged; conversely, if \mathbf{X}_k^s is rejected, \mathbf{X}_k remains as \mathbf{X}_{k+1} , and Δ_k is reduced to enable the construction of a more accurate local model.

As described in Section 3.2, our proposed algorithm executes the aforementioned four steps multiple times within a single iteration to address Q1, utilizing both HF and LF simulation oracles. Specifically, when a strong correlation between the LF and HF function is estimated within the TR based on the optimization history, the local model are first constructed for the LF function. If the LF-based local model fails to produce a candidate with a lower HF objective estimate, a local model for the HF function is then constructed.

1.4 Summary of Results and Insight.

In this paper, we propose a novel stochastic TR method, which employs two separate TRs to handle HF and LF functions, and incorporates an adaptive sampling scheme specifically designed for BFSO, named ASTRO-BFDF. Our key contributions are as follows:

- (a) Addressing Q1, we introduce an adaptive correlation constant (α_k in Algorithm 2), capturing local correlation between the HF and LF functions.
- (b) Addressing Q2, we suggest a new adaptive sampling algorithm, named BFAS, which leverages both HF and LF oracles and dynamically controls n, v , and c through updates from each new sample.
- (c) We prove the almost sure convergence, i.e., $\lim_{k \rightarrow \infty} \|\nabla f^h(\mathbf{X}_k)\| = 0$ w.p.1, of ASTRO-BFDF.
- (d) Extensive numerical experiments demonstrate that ASTRO-BFDF consistently outperforms a range of bi-fidelity and single-fidelity solvers across varying correlation levels between the HF and LF functions, as well as different variances of HF and LF stochastic noise.

2 Preliminaries

In this section, we provide key definitions, standing assumptions, and some useful results that will be invoked in the convergence analysis of the proposed algorithm.

2.1 Notation

We represent vectors using bold font; for instance, $\mathbf{x} = (x_1, x_2, \dots, x_d) \in \mathbb{R}^d$ refers to a vector in d -dimensional space. Sets are denoted with calligraphic fonts, while matrices are shown in sans serif fonts. The default norm, $\|\cdot\|$, is the ℓ_2 norm. The closed ball of radius $\Delta > 0$ centered at \mathbf{x}^0 is $\mathcal{B}(\mathbf{x}^0; \Delta) = \{\mathbf{x} \in \mathbb{R}^d : \|\mathbf{x} - \mathbf{x}^0\| \leq \Delta\}$. For a sequence of sets $\mathcal{A}_n, \mathcal{A}_n$ i.o. denotes $\limsup_{n \rightarrow \infty} \mathcal{A}_n$, where ‘‘i.o.’’ stands for ‘‘infinitely often.’’ We write $f(\mathbf{x}) = \mathcal{O}(g(\mathbf{x}))$ if there are positive constants ε and m such that $|f(\mathbf{x})| \leq mg(\mathbf{x})$ for all \mathbf{x} with $0 < \|\mathbf{x}\| < \varepsilon$. Capital letters denote random scalars and vectors. For a sequence of random vectors $\{\mathbf{X}_k, k \geq 1\}$, $\mathbf{X}_k \xrightarrow{w.p.1} \mathbf{X}$ denotes almost sure convergence. ‘‘iid’’ means independent and identically distributed, and ‘‘w.p.1’’ means with probability 1. The superscripts h and l indicate that the terminology is related to high-fidelity and low-fidelity simulations, respectively. The terms $\hat{\sigma}^h(\mathbf{x}, n)$ and $\hat{\sigma}^l(\mathbf{x}, n)$ are the standard deviation estimates of HF and LF functions at \mathbf{x} with sample size n , while $\hat{\sigma}^{h,l}(\mathbf{x}, n)$ is the covariance estimate between them.

2.2 Key Definitions

We introduce the definition of a stochastic interpolation model, used as the local model in ASTRO-BFDF.

Definition 1 (stochastic interpolation models: Definition 2.3 in [24]). *Given $\mathbf{X}_k = \mathbf{X}_k^0 \in \mathbb{R}^d$ and $\Delta_k^q > 0$, let $\Phi(\mathbf{x}) = [\phi_0(\mathbf{x}), \phi_1(\mathbf{x}), \dots, \phi_p(\mathbf{x})]$ be a polynomial basis on \mathbb{R}^d . With $p = d(d+3)/2$, $q \in \{h, l\}$ and the design set $\mathcal{X}_k = \{\mathbf{X}_k^i\}_{i=0}^p \subset \mathcal{B}(\mathbf{X}_k; \Delta_k^q)$, we find $\boldsymbol{\nu}_k^q = [\nu_{k,0}^q, \nu_{k,1}^q, \dots, \nu_{k,p}^q]^\top$ such that*

$$\mathbf{M}(\Phi, \mathcal{X}_k) \boldsymbol{\nu}_k^q = [\bar{F}_k^q(\mathbf{X}_k^0, N(\mathbf{X}_k^0)), \bar{F}_k^q(\mathbf{X}_k^1, N(\mathbf{X}_k^1)), \dots, \bar{F}_k^q(\mathbf{X}_k^p, N(\mathbf{X}_k^p))]^\top, \quad (5)$$

where

$$\mathbf{M}(\Phi, \mathcal{X}_k) = \begin{bmatrix} \phi_1(\mathbf{X}_k^0) & \phi_2(\mathbf{X}_k^0) & \cdots & \phi_p(\mathbf{X}_k^0) \\ \phi_1(\mathbf{X}_k^1) & \phi_2(\mathbf{X}_k^1) & \cdots & \phi_p(\mathbf{X}_k^1) \\ \vdots & \vdots & \vdots & \vdots \\ \phi_1(\mathbf{X}_k^p) & \phi_2(\mathbf{X}_k^p) & \cdots & \phi_p(\mathbf{X}_k^p) \end{bmatrix}.$$

We say \mathcal{X}_k is poised provided $\mathsf{M}(\Phi, \mathcal{X}_k)$ is nonsingular. If there exists a solution to (5), then the function $M_k^q : \mathcal{B}(\mathbf{X}_k; \Delta_k^q) \rightarrow \mathbb{R}$, defined as $M_k^q(\mathbf{x}) = \sum_{j=0}^p \nu_{k,j}^q \phi_j(\mathbf{x})$ is a stochastic polynomial interpolation of estimated values of f^q on $\mathcal{B}(\mathbf{X}_k; \Delta_k^q)$. In particular, if $\mathbf{G}_k^q = [\nu_{k,1}^q \ \nu_{k,2}^q \ \cdots \ \nu_{k,d}^q]^\top$ and \mathbf{H}_k^q is a symmetric $d \times d$ matrix with elements uniquely defined by $(\nu_{k,d+1}^q, \nu_{k,d+2}^q, \dots, \nu_{k,p}^q)$, then we can define the stochastic quadratic model $M_k^q : \mathcal{B}(\mathbf{X}_k; \Delta_k^q) \rightarrow \mathbb{R}$, as

$$M_k^q(\mathbf{x}) = \nu_{k,0}^q + (\mathbf{x} - \mathbf{X}_k)^\top \mathbf{G}_k^q + \frac{1}{2}(\mathbf{x} - \mathbf{X}_k)^\top \mathbf{H}_k^q(\mathbf{x} - \mathbf{X}_k). \quad (6)$$

The next definition states that the approximate solution to the subproblem in ASTRO-BFDF ensures a sufficient decrease in the local model (see Theorem 10.1 in [33]).

Definition 2 (Cauchy reduction: Definition 2.5 in [24]). *Given $\mathbf{X}_k \in \mathbb{R}^d$, $\Delta_k^q > 0$, $q \in \{h, \ell\}$, and a function $M_k^q : \mathcal{B}(\mathbf{X}_k; \Delta_k^q) \rightarrow \mathbb{R}$ obtained following Definition 1, \mathbf{S}_k^c is called the Cauchy step if*

$$M^q(\mathbf{X}_k) - M^q(\mathbf{X}_k + \mathbf{S}_k^c) \geq \frac{1}{2} \|\nabla M^q(\mathbf{X}_k)\| \min \left\{ \frac{\|\nabla M^q(\mathbf{X}_k)\|}{\|\nabla^2 M^q(\mathbf{X}_k)\|}, \Delta_k^q \right\}.$$

When $\|\nabla^2 M_k^q(\mathbf{X}_k)\| = 0$, we assume $\|\nabla M^q(\mathbf{X}_k)\|/\|\nabla^2 M^q(\mathbf{X}_k)\| = +\infty$. The Cauchy step is derived by minimizing the model $M_k^q(\cdot)$ along the steepest descent direction within $\mathcal{B}(\mathbf{X}_k; \Delta_k^q)$, making it easy and quick to compute.

Lastly, we introduce the concepts of filtration and stopping time, which play a crucial role in analyzing the behavior of ASTRO-BFDF and BFAS.

Definition 3 (filtration and stopping time: Section 35 in [34]). *A filtration $\{\mathcal{F}_k\}_{k \geq 1}$ on a probability space $(\Omega, \mathbb{P}, \mathcal{F})$ is a sequence of σ -algebras, each contained within the next, such that for all k , \mathcal{F}_k is a subset of \mathcal{F}_{k+1} , and all are subsets of \mathcal{F} . A function $N : \Omega \rightarrow \{0, 1, 2, \dots, \infty\}$ is referred to as a stopping time with respect to the filtration \mathcal{F} if the set $\{\omega \in \Omega : N(\omega) = n\}$ is an element of \mathcal{F} for every $n < \infty$.*

2.3 Standing Assumptions

We now state the standing assumptions underlying our analysis. Assumption 1 specifies the characteristics of the functions f^h and f^ℓ , which precisely define the problem under consideration.

Assumption 1 (function). *The HF function f^h and the LF function f^ℓ are continuously differentiable in an open domain Ω , ∇f^h and ∇f^ℓ are Lipschitz continuous in Ω with constant $\kappa_{Lg} > 0$.*

We make the next assumption on the higher moments of the stochastic noise following a Bernstein-type condition adapted to a martingale setting. Random variables fulfilling Assumption 2 exhibit a subexponential tail behavior.

Assumption 2 (stochastic noise). *The Monte Carlo oracles generate iid random variables $F^q(\mathbf{X}_k^i, \xi_j^q) = f^q(\mathbf{X}_k^i) + E_{k,j}^{i,q}$ with $E_{k,j}^{i,q} \in \mathcal{F}_{k,j}$ for $i \in \{0, 1, 2, \dots, p, s\}$ and $q \in \{h, \ell\}$, where \mathbf{X}_k^s is the candidate iterate at iteration k and $\mathcal{F}_k = \mathcal{F}_{k,0} \subset \mathcal{F}_{k,1} \subset \dots \subset \mathcal{F}_{k+1}$ for all k . Then the stochastic errors*

$E_{k,j}^{i,q}$ are independent of \mathcal{F}_{k-1} , $\mathbb{E}[E_{k,j}^{i,q} \mid \mathcal{F}_{k,j-1}] = 0$, and there exists $(\sigma^q)^2 > 0$ and $b^q > 0$ such that for a fixed n ,

$$\frac{1}{n} \sum_{j=1}^n \mathbb{E}[|E_{k,j}^{i,q}|^m \mid \mathcal{F}_{k,j-1}] \leq \frac{m!}{2} (b^q)^{m-2} (\sigma^q)^2, \quad \forall m = 2, 3, \dots, \forall k. \quad (7)$$

2.4 Useful Results

In this section, we present useful results that will be invoked to prove the almost sure convergence of ASTRO-BFDF. We begin by introducing Bernsetin inequality for martingales.

Lemma 1 (Bernsetin inequality for martingales: Lemma 2.5 by [35]). *Let $(\xi_i, \mathcal{F}_i)_{i=0,1,\dots}$ be a martingale difference sequence on some probability space (Ω, \mathcal{F}, P) with $\mathbb{E}[\xi_i \mid \mathcal{F}_{i-1}] = 0$, where $\xi_0 = 0$ and $\{\Omega, \emptyset\} = \mathcal{F}_0 \subseteq \mathcal{F}_1 \subseteq \mathcal{F}_2 \subseteq \dots \subseteq \mathcal{F}_n \subseteq \mathcal{F}$ is a sequence of increasing filtrations. Furthermore, assume that there exist constants $b > 0$ and $\sigma_\xi^2 > 0$ such that for any $m \in \{2, 3, \dots\}$, and any $i \in \{0, 1, \dots\}$,*

$$\mathbb{E}[|\xi_i|^m \mid \mathcal{F}_{i-1}] \leq \frac{1}{2} m! b^{m-2} \sigma_\xi^2.$$

Then, for any $c > 0$ and any $n \in \mathbb{N}$,

$$\mathbb{P}\left\{\sum_{i=1}^n \xi_i \geq nc\right\} \leq \exp\left\{-\frac{nc^2}{2(bc + \sigma_\xi^2)}\right\}.$$

The next result demonstrates that, under Assumption 2, the estimate of the stochastic errors is bounded by the square of the TR radius when a specific adaptive sampling rule is applied. This result matches the guaranteed estimation accuracy given by $\mathbb{P}\{|N(\mathbf{X}_k^i)^{-1} \sum_{j=1}^{N(\mathbf{X}_k^i)} E_{k,j}^{i,q}| \geq c_f(\Delta_k^q)^2\} \leq \alpha_k$ for any given $c_f > 0$, where α_k increases gradually, driven by a logarithmically increasing sequence λ_k . This type of inflation factor is a common approach in sequential estimation settings [36].

Theorem 1 (Stochastic noise: Theorem 3.2 with case (A-0) by [35]). *Let $c_f > 0$ and $\Delta_k^q > 0$ be given and $E_{k,j}^{i,q}$ denotes the stochastic noise following Assumption 2. Given any $\epsilon_\lambda \in (0, 1)$ and $\lambda_0 \geq 2$, suppose the adaptive sample size $N(\mathbf{X}_k^i)$ is a stopping time satisfying $N(\mathbf{X}_k^i) \geq (\sigma_0^q)^2 \lambda_k \kappa^{-2} (\Delta_k^q)^{-4}$, where $\sigma_0 > 0$, $\kappa > 0$, and $\lambda_k = \lambda_0 (\log k)^{1+\epsilon_\lambda}$. Then, the following series is summable:*

$$\sum_{k=1}^{\infty} \mathbb{P}\left\{\left|\frac{1}{N(\mathbf{X}_k^i)} \sum_{j=1}^{N(\mathbf{X}_k^i)} E_{k,j}^{i,q}\right| \geq c_f(\Delta_k^q)^2\right\} < \infty.$$

Although Theorem 1 has been proven with the following adaptive sampling rule (See Section 3.2 of [35])

$$N(\mathbf{X}_k^i) = \min\left\{n \in \mathbb{N} : \frac{\max\{\sigma_0, \hat{\sigma}^h(\mathbf{X}_k^i, n)\}}{\sqrt{n}} \leq \frac{\kappa(\Delta_k^q)^2}{\sqrt{\lambda_k}}\right\}, \quad (8)$$

it can also be trivially established with a stopping time $N(\mathbf{X}_k^i) \geq \mathcal{O}(\lambda_k(\Delta_k^q)^{-4})$ by employing the same logical framework. The detailed proof is provided in Appendix A. The next result provides an upper bound for the gradient error norm at any design point within the TR when a stochastic linear or quadratic interpolation model is used. Combined with Theorem 1, it indicates that the gradient error norm will be bounded by the order of the TR radius after sufficiently many iterations.

Lemma 2 (Stochastic Interpolation Model: Lemma 2.9 by [24]). *Let Assumptions 1 and 2 hold. If $M_k^q(\mathbf{z})$ is a stochastic linear interpolation model or a stochastic quadratic interpolation model of f^q with the design set $\mathcal{X}_k = \{\mathbf{X}_k^i\}_{i=0}^p \subset \mathcal{B}(\mathbf{X}_k; \Delta_k^q)$ and corresponding function estimates $\bar{F}^q(\mathbf{X}_k^i, N(\mathbf{X}_k^i)) = f^q(\mathbf{X}_k^i) + \bar{E}_k^{i,q}(N_k^i)$, there exist positive constants κ_{eg1} and κ_{eg2} such that for any $\mathbf{z} \in \mathcal{B}(\mathbf{X}_k; \Delta_k^q)$,*

$$\|\nabla M^q(\mathbf{z}) - \nabla f^q(\mathbf{z})\| \leq \kappa_{eg1} \Delta^q + \kappa_{eg2} \frac{\sqrt{\sum_{i=1}^p (\bar{E}_k^{i,q}(N_k^i) - \bar{E}_k^{0,q}(N_k^0))}}{\Delta^q}, \quad (9)$$

where $\bar{E}_k^{i,q}(N_k^i) = N(\mathbf{X}_k^i)^{-1} \sum_{j=1}^{N(\mathbf{X}_k^i)} E_{k,j}^{i,q}$.

Lastly, we present the variance of BFMC estimator under the Common Random Numbers (CRN) scheme. In the CRN setting, the same stochastic realization ω_i drives both HF and LF simulations, yielding paired samples ξ_i^h and ξ_i^ℓ . The induced positive correlation reduces the variance of the BFMC function estimates and the estimated function reductions between successive design points.

Lemma 3 (Variance of BFMC under CRN: Lemma 3.3 by [26]). *Let $E_{k,j}^{i,q}$ denote the stochastic noise satisfying Assumption 2. The index j corresponds to the j -th common random number ω_j , so the pair $(E_{k,j}^{i,h}, E_{k,j}^{i,\ell})$ shares the same realization and has covariance $\sigma^{h,\ell}(\mathbf{X}_k^i) = \text{Cov}(E_{k,j}^{i,h}, E_{k,j}^{i,\ell})$. Then the variance of the BFMC estimator $\bar{F}^{\text{bf}}(\mathbf{X}_k^i, n, v, c)$ is*

$$\begin{aligned} \text{Var}(\bar{F}^{\text{bf}}(\mathbf{X}_k^i, n, v, c)) &= \frac{(\sigma^h(\mathbf{X}_k^i))^2}{n} + c^2 \left(\frac{1}{n} - \frac{1}{v} \right) (\sigma^\ell(\mathbf{X}_k^i))^2 \\ &\quad + 2c \left(\frac{1}{v} - \frac{1}{n} \right) \sigma^{h,\ell}(\mathbf{X}_k^i), \end{aligned} \quad (10)$$

for any $n, v \in \mathbb{N}$ with $n < v$, $c \in \mathbb{R}$, and $i \in \{0, 1, \dots, p, s\}$.

We note that (4) is identical to (10) under Assumption 2 with CRN, since $\text{Cov}(\bar{F}^h(\mathbf{X}_k^i, n), \bar{F}^\ell(\mathbf{X}_k^i, v)) = (\max\{n, v\})^{-1} \sigma^{h,\ell}(\mathbf{X}_k^i)$ and $\text{Var}(\bar{F}^q(\mathbf{X}_k^i, n)) = n^{-1} (\sigma^q(\mathbf{X}_k^i))^2$ for any $q \in \{h, \ell\}$ (see Lemma 3.2 by [26]). Since $\sigma^h(\mathbf{X}_k^i)$, $\sigma^\ell(\mathbf{X}_k^i)$, and $\sigma^{h,\ell}(\mathbf{X}_k^i)$ are usually unknown in reality, we use their empirical estimates, such as $\hat{\sigma}^h(\mathbf{X}_k^i, n)$, $\hat{\sigma}^\ell(\mathbf{X}_k^i, v)$, and $\hat{\sigma}^{h,\ell}(\mathbf{X}_k^i, n)$. Using these estimates in place of the true values does not affect the convergence of ASTRO-BFDF, but instead represents a more realistic implementation of the sampling scheme in practice. Lastly, we present Borel-Cantelli's First Lemma for martingales that repeatedly invoke.

Lemma 4 (Borel-Cantelli for martingales: Chapter 12.15 in [37]). *Let $\{A_n\}_{n \geq 1}$ be a sequence of events on a probability space $(\Omega, \mathcal{F}, \mathbb{P})$, and let $\{\mathcal{F}_n\}$ be a filtration. If $\sum_{n=1}^{\infty} \mathbb{P}(A_n \mid \mathcal{F}_{n-1}) < \infty$ a.s., then $\mathbb{P}(A_n \text{ i.o.}) = 0$.*

3 Adaptive Sampling Bi-fidelity Trust Region Optimization

Similar to other stochastic TR algorithms, our proposed adaptive sampling bi-fidelity TR algorithm (ASTRO-BFDF), which build upon ASTRO-DF [24], generates the sequence $\{\mathbf{X}_k\}$ through the four steps outlined in Section 1.3. ASTRO-BFDF differs from ASTRO-DF in two key components, primarily due to the presence of an LF simulation oracle:

- (1) Sample sizes are carefully managed through adaptive sampling using BFMC or CMC. Within this approach, two critical decisions are made. First, as samples are collected, the algorithm determines whether to employ CMC or BFMC. Second, it dynamically adjusts the sample sizes for both HF and LF simulation oracles and determines the coefficient c in (3), all in real time as sampling progresses.
- (2) At each iteration k , two local models can be constructed using HF and LF simulation oracles, each associated with its own TR: Δ_k^ℓ for the LF function and Δ_k^h for the HF function. The LF-based local model serves two purposes: (i) identifying a candidate solution for the next iterate, and (ii) updating the adaptive correlation constant (α_k in Algorithm 2 and 3).

We first introduce the bi-fidelity adaptive sampling (BFAS) strategy, which corresponds to the first feature.

3.1 Adaptive Sampling for Bi-Fidelity Stochastic Optimization

While BFMC can reduce the variance of function estimates, blindly employing BFMC may not always be advantageous. For example, when the inherent variance of the LF simulation significantly exceeds that of the HF simulation, a substantial number of LF samples are required to reduce BFMC variance (see Lemma 3). In such cases, if the LF oracle is only marginally cheaper than the HF oracle, the cost advantage of BFMC diminishes, making CMC potentially more efficient. Therefore, it is essential to determine which Monte Carlo method to employ at a given design point based on the variance of the LF and HF simulation outputs and the covariance between them. However, the true variances of the HF and LF simulations and their covariance are unknown. Consequently, when adaptive sampling is used, the choice of the MC method needs to be dynamically determined based on variance and covariance estimates, which are sequentially updated from simulation results. In summary, it is necessary to dynamically determine N, V , and C while collecting simulation replications, where N and V are the sample sizes for the HF and LF oracles and C represents the coefficient in the BFMC estimate, (denoted as c in (3)). To achieve this for any $\mathbf{x} \in \mathbb{R}^d$ at iteration k , we suggest BFAS, as listed in Algorithm 1.

Algorithm 1 starts by sampling n HF oracle calls and v LF oracle calls to estimate the variance and covariance terms in (4). Using the variance estimate $\hat{\sigma}^h(\mathbf{x}, n)$, we compute a predicted minimum sample size $N^p(\mathbf{x})$ for CMC, adhering to the adaptive sampling rule (8). Then the predicted computational cost of CMC at \mathbf{x} is $w^h N^p(\mathbf{x})$, where w^h is the cost of one HF oracle call. Next, this cost is compared to the projected computational cost of BFMC. To predict the minimum cost for BFMC, we solve (12) using the variance estimates $\hat{\sigma}^h(\mathbf{x}, n)$, $\hat{\sigma}^\ell(\mathbf{x}, v)$, and $\hat{\sigma}^{h,\ell}(\mathbf{x}, n)$ for $\text{Var}(\bar{F}^{\text{bf}}(\mathbf{x}, \tilde{n}, \tilde{v}, \tilde{c}))$ (See Lemma 3).

$$\begin{aligned}
[N^*, V^*, C^*] \in \operatorname{argmin}_{\tilde{n}, \tilde{v}, \tilde{c} \in \mathbb{R}} \quad & w^h \tilde{n} + w^\ell \tilde{v} \\
\text{subject to} \quad & \text{Var}(\bar{F}^{\text{bf}}(\mathbf{x}, \tilde{n}, \tilde{v}, \tilde{c})) \leq \kappa^2 \Delta_k^4 \lambda_k^{-1} \\
& \tilde{n} - \tilde{v} \leq 0 \\
& n \leq \tilde{n} \leq \infty \\
& v \leq \tilde{v} < \infty,
\end{aligned} \tag{12}$$

where w^ℓ is the cost of a single LF oracle call. The first constraint corresponds to the adaptive sampling rule from (8), ensuring that the BFMC estimator achieves the required accuracy. Problem (12) is a three-dimensional deterministic continuous optimization problem that can be

Algorithm 1 $[N_k(\mathbf{x}), V_k(\mathbf{x}), C_k(\mathbf{x}), \tilde{F}_k(\mathbf{x})] = \text{BFAS}(\mathbf{x}, \Delta_k, \lambda_k, \kappa, s^h, s^\ell, w^h, w^\ell)$

Input: $\mathbf{x} \in \mathbb{R}^d$, TR radius Δ_k , sample size lower bound sequence $\{\lambda_k\}$, batch size $s^h < s^\ell$ for HF and LF oracles, adaptive sampling constant $\kappa > 0$, lower bound of an initial variance approximation $\sigma_0 > 0$, and costs $w^h \geq w^\ell$ of calling HF and LF oracles.

Output: HF sample size $N_k(\mathbf{x})$, LF sample size $V_k(\mathbf{x})$, MFMC coefficient $C_k(\mathbf{x})$, and function estimate $\tilde{F}_k(\mathbf{x})$

- 1: Set $n = (\sigma_0)^2 \lambda_k (\kappa^2 \Delta_k^4)^{-1}$ and $v = n + 1$.
- 2: Estimate $\hat{\sigma}^h(\mathbf{x}, n)$, $\hat{\sigma}^{h,\ell}(\mathbf{x}, n)$, and $\hat{\sigma}^\ell(\mathbf{x}, v)$.
- 3: Obtain the CMC-predicted sample sizes $N^p(\mathbf{x})$, where

$$N^p(\mathbf{x}) = \min \left\{ n^p \in \mathbb{N} : \frac{\hat{\sigma}^h(\mathbf{x}, n)}{\sqrt{n^p}} \leq \frac{\kappa \Delta_k^2}{\sqrt{\lambda_k}} \right\} \quad (11)$$

- 4: **loop**
- 5: Approximately compute C^* , N^* , and V^* by solving the problem (12) and set $c = C^*$.
- 6: **if** $w^h N^* + w^\ell V^* \leq w^h N^p(\mathbf{x})$ **then**
- 7: Set $v = \max\{n + 1, v\}$ and update $\hat{\sigma}^{h,\ell}(\mathbf{x}, n)$ and $\hat{\sigma}^\ell(\mathbf{x}, v)$ by calling the LF oracle.
- 8: **if** $\text{Var}(\bar{F}^{\text{bf}}(\mathbf{x}, n, v, c)) \leq \kappa^2 \Delta_k^4 \lambda_k^{-1}$ (Condition 1) **then**
- 9: **return** $[n, v, c, \bar{F}^{\text{bf}}(\mathbf{x}, n, v, c)]$ (BFMC)
- 10: **end if**
- 11: **if** $n \geq N^* - 1$ **then**
- 12: Set $v = v + s^\ell$ and get s^ℓ additional replications of the LF oracle and update $\tilde{\sigma}^\ell(\mathbf{x}, v)$.
- 13: **else**
- 14: Set $n = n + s^h$ and update $\hat{\sigma}^h(\mathbf{x}, n)$ and $\hat{\sigma}^{h,\ell}(\mathbf{x}, n)$ by calling the LF and HF oracles.
- 15: **end if**
- 16: **else**
- 17: **if** $n \geq N^p(\mathbf{x})$ (Condition 2) **then**
- 18: **if** $\text{Var}(\bar{F}^{\text{bf}}(\mathbf{x}, n, v, c)) \leq \text{Var}(\bar{F}^h(\mathbf{x}, n))$ and $n < v$ **then**
- 19: **return** $[n, v, c, \bar{F}^{\text{bf}}(\mathbf{x}, n, v, c)]$ (MFMC)
- 20: **else**
- 21: **return** $[n, v, c, \bar{F}^h(\mathbf{x}, n)]$ (CMC)
- 22: **end if**
- 23: **end if**
- 24: Set $n = n + s^h$ and update $\hat{\sigma}^h(\mathbf{x}, n)$ and $N^p(\mathbf{x})$ by calling the HF oracle.
- 25: **end if**
- 26: **end loop**

efficiently solved in practice. We next compare the predicted computational costs between CMC and BFMC.

If the predicted cost of BFMC is lower than that of CMC, BFMC is expected to be more cost-effectiveness, and the algorithm proceeds to Step 7. We first set $v = \max\{v, n + 1\}$ with the updated n in Step 24 to ensure that $v > n$. Following this adjustment, additional LF oracle replications may be required, and we update both $\hat{\sigma}^l(\mathbf{x}, v)$ and $\hat{\sigma}^{h,\ell}(\mathbf{x}, n)$ accordingly. Next, if the variance of the BFMC estimator satisfies the accuracy condition , i.e.,

$$\text{Var}(\bar{F}^{\text{bf}}(\mathbf{x}, n, v, c)) \leq \kappa^2 \Delta_k^4 \lambda_k^{-1}, \quad (13)$$

the algorithm returns $\bar{F}^{\text{bf}}(\mathbf{x}, n, v, c)$. Otherwise, the algorithm determines whether to increase n or v . Since n has a stronger effect on reducing the variance, the algorithm first checks whether $n < N^* - 1$. If so, n is increased by s^h , and the relevant variance and covariance estimates are updated. If $n \geq N^* - 1$, additional LF oracle samples are obtained, and $\hat{\sigma}^\ell(\mathbf{x}, v)$ is updated. The algorithm then returns to Step 5.

After solving the subproblem, if the projected cost of achieving the required accuracy using CMC is lower than that of BFMC, the algorithm switches to CMC to avoid unnecessary LF sampling. If $n \geq N^p$, the function estimate is sufficiently accurate for optimization, and the algorithm returns the estimator (CMC or BFMC) with the lower estimated variance, ensuring the most accurate result. If not, n is increased, the variance estimate is updated, and the process continues. Note that the LF variance estimate and covariance estimate are not updated at this stage.

Since n, v , and c are dynamically determined based on simulation realizations, three outputs of BFAS are the stopping times determined by the filtration. Hence, we refer the output of Algorithm 1 as $[N_k(\mathbf{x}), V_k(\mathbf{x}), C_k(\mathbf{x}), \tilde{F}_k(\mathbf{x})]$.

Remark 1 (Computational Costs of BFAS). *The total cost of BFAS is given by $w^h N_k(\mathbf{x}) + w^\ell V_k(\mathbf{x})$. If either Condition 1 or Condition 2 is met based on the initial estimates, this cost reduces to $w^h n + w^\ell v$, which represents the minimum possible cost. If the final output is the BFMC estimate, the computational cost is strictly lower than that of CMC because of Step 6. Conversely, when the output is CMC, the $V_k(\mathbf{x})$ LF replications do not contribute to the final estimate. The adaptive sampling scheme mitigates this redundancy by ensuring that only the HF oracle is called when CMC appears more cost-effective but Condition 2 is not yet satisfied (Step 24 in Algorithm 1). Furthermore, LF oracle replications are reused to construct the LF-based local model, as detailed in Section 3.2.*

3.2 Bi-fidelity Stochastic Trust Region Method

We now delve into the bi-fidelity stochastic TR method with adaptive sampling (ASTRO-BFDF). The core idea of ASTRO-BFDF is to primarily exploit the LF oracle until it no longer yields a solution that improves upon the current incumbent solution. Hence, unlike the stochastic TR methods discussed in Section 1.3, ASTRO-BFDF constructs two local models within separate TRs tailored to the HF and LF functions, denoted by Δ_k^h and Δ_k^ℓ , respectively. Note that Δ_k^h is always larger than Δ_k^ℓ for all iterations to maintain large steps for the HF-based local model and save computational budget in (11) and (13).

With two TRs, it is essential to determine when and how to construct the LF-based local model, as uncontrolled use of the LF oracle can lead to inefficiency [21]. The main difficulty is assessing the local usefulness of the LF model for optimization without performing costly global comparisons with the HF model. Previous studies have attempted to address this by quantifying the correlation between the HF and LF functions through sampling various design points and their corresponding function estimates [38, 39, 40]. However, as will be shown in Section 5, low global correlation does not always mean that the LF function is unhelpful for optimization. In the TR method, it is necessary to ascertain the utility of the LF oracle within the TR rather than across the entire domain. Therefore, we introduce an adaptive correlation constant, α_k , to decide whether constructing the LF-based local model M_k^ℓ is worthwhile.

The adaptive correlation constant is dynamically updated leveraging results from previous iterations, similar to the TR radius. This enables the algorithm to evaluate whether the LF

Algorithm 2 ASTRO-BFDF

Input: Initial incumbent $\mathbf{x}_0 \in \Re^d$, initial and maximum TR radius $\Delta_0^\ell, \Delta_0^h, \Delta_{\max} > 0$, model fitness thresholds $0 < \eta < 1$ and certification threshold $\mu > 0$, expansion and shrinkage constants $\gamma_1 > 1$ and $\gamma_2 \in (0, 1)$, sample size lower bound sequence $\{\lambda_k\} = \{\mathcal{O}(\log k)\}$, adaptive sampling constant $\kappa > 0$, correlation constant $\alpha_k > 0$, and lower bound of an initial variance approximation $\sigma_0 > 0$, and sufficient reduction constant $\zeta > 0$.

Output: Solution sequence $\{\mathbf{X}_k\}$

```

1: for  $k = 0, 1, 2, \dots$  do
2:   Set  $I_k^h = \text{True}$ .
3:   while  $\alpha_k < \alpha_{th}$  do
4:     Obtain  $\check{\mathbf{X}}_k^\ell$  and  $I_k^h$  by calling Algorithm 3.
5:     if  $I_k^h$  is True then
6:       Set  $\Delta_k^\ell = \gamma_2 \Delta_k^\ell$  and  $\alpha_k = \gamma_2 \alpha_k$ 
7:     else
8:       Set  $(\mathbf{X}_{k+1}, \Delta_{k+1}^\ell) = (\check{\mathbf{X}}_k^\ell, \gamma_1 \Delta_k^\ell)$  and  $\alpha_{k+1} = \min\{\gamma_1 \alpha_k, 1\}$ .
9:       Set  $\Delta_{k+1}^h = \max\{\Delta_{k+1}^\ell, \Delta_k^h\}$  and  $k = k + 1$ .
10:      break
11:    end if
12:   end while
13:   if  $I_k^h$  is True then
14:     Select  $\mathcal{X}_k = \{\mathbf{X}_k^i\}_{i=0}^{2d} \subset \mathcal{B}(\mathbf{X}_k; \Delta_k^h)$ .
15:     Estimate the HF function at  $\{\mathbf{X}_k^i\}_{i=0}^{2d}$  by calling Algorithm 1 with  $\Delta_k = \Delta_k^h$ .
16:     Estimate the LF function  $\bar{F}^\ell(\mathbf{X}_k^i, T_k^i)$  at  $\{\mathbf{X}_k^i\}_{i=0}^{2d}$ , satisfying

```

$$T_k^i = \min \left\{ t \in \mathbb{N} : \frac{\max\{\sigma_0, \hat{\sigma}^\ell(\mathbf{X}_k^i, t)\}}{\sqrt{t}} \leq \frac{\kappa(\Delta_k^h)^2}{\sqrt{\lambda_k}} \right\}. \quad (14)$$

```

17:   Construct local models  $M_k^\ell(\mathbf{X})$  and  $M_k^h(\mathbf{X})$ .
18:   Approximately compute the local model minimizers

```

$$\mathbf{X}_k^{s,h} \in \underset{\|\mathbf{X} - \mathbf{X}_k\| \leq \Delta_k^h}{\operatorname{argmin}} M_k^h(\mathbf{X}) \text{ and } \mathbf{X}_k^{s,\ell} \in \underset{\|\mathbf{X} - \mathbf{X}_k\| \leq \Delta_k^h}{\operatorname{argmin}} M_k^\ell(\mathbf{X}).$$

```

19:   Estimate  $\tilde{F}(\mathbf{X}_k^{s,h})$  and  $\tilde{F}(\mathbf{X}_k^{s,\ell})$  by calling Algorithm 1 with  $\Delta_k = \Delta_k^h$ .
20:   Set the candidate point  $\mathbf{X}_k^s \in \operatorname{argmin}_{\mathbf{x} \in \{\mathbf{X}_k^{s,h}, \mathbf{X}_k^{s,\ell}\}} \tilde{F}(\mathbf{x})$ .
21:   Compute the success ratio  $\hat{\rho}_k$  and  $\hat{\rho}_k^\ell$  as

```

$$\hat{\rho}_k = \frac{\tilde{F}_k(\mathbf{X}_k^0) - \tilde{F}_k(\mathbf{X}_k^{s,h})}{M_k^h(\mathbf{X}_k^0) - M_k^h(\mathbf{X}_k^{s,h})} \text{ and } \hat{\rho}_k^\ell = \frac{\tilde{F}_k(\mathbf{X}_k^0) - \tilde{F}_k(\mathbf{X}_k^{s,\ell})}{\max\{\zeta(\Delta_k^h)^2, M_k^h(\mathbf{X}_k^0) - M_k^h(\mathbf{X}_k^{s,\ell})\}}.$$

```

22:   If  $\hat{\rho}_k^\ell \geq \eta$ , set  $\alpha_{k+1} = \gamma_1 \alpha_k$ ; otherwise set  $\alpha_{k+1} = \gamma_2 \alpha_k$ .
23:   Set  $(\mathbf{X}_{k+1}, \Delta_{k+1}^h) =$ 

```

$$\begin{cases} (\mathbf{X}_k^s, \min\{\gamma_1 \Delta_k^h, \Delta_{\max}\}) & \text{if } \hat{\rho}_k \geq \eta \text{ and } \mu \|\nabla M_k^h(\mathbf{X}_k)\| \geq \Delta_k^h, \\ (\mathbf{X}_k, \gamma_2 \Delta_k^h) & \text{otherwise,} \end{cases}$$

```

24:   end if
25: end for


---



```

Algorithm 3 $[\check{\mathbf{X}}_k^\ell, I_k^h] = \text{ASTRO-LFDF}(\mathbf{X}_k)$

Input: $\mathbf{X}_k, \Delta_k^\ell$, model fitness thresholds $0 < \eta < 1$ and certification threshold $\mu > 0$, sufficient reduction constant $\theta > 0$, expansion and shrinkage constants $\gamma_1 > 1$ and $\gamma_2 \in (0, 1)$, sample size lower bound sequence $\{\lambda_k\} = \{\mathcal{O}(\log k)\}$, adaptive sampling constant $\kappa > 0$, correlation constant $\alpha_k > 0$, correlation threshold $\alpha_{th} > 0$, lower bound of an initial variance approximation $\sigma_0 > 0$, and sufficient reduction constant $\zeta > 0$.

Output: candidate solution $\check{\mathbf{X}}_k^\ell$ and indicator I_k^h for HF-based local model construction.

- 1: Select $\mathcal{X}_k^\ell = \{\mathbf{X}_k^i\}_{i=0}^p \subset \mathcal{B}(\mathbf{X}_k; \Delta_k^\ell)$.
- 2: Estimate $\bar{F}^\ell(\mathbf{X}_k^i, T_k^i)$ at $\{\mathbf{X}_k^i\}_{i=0}^{2d}$, satisfying (14) with Δ_k^ℓ instead Δ_k^h .
- 3: Construct local model $M_k^\ell(\mathbf{X})$.
- 4: Approximately compute the local model minimizer

$$\mathbf{X}_k^{s,\ell} = \underset{\|\mathbf{X} - \mathbf{X}_k\| \leq \Delta_k^\ell}{\operatorname{argmin}} M_k^\ell(\mathbf{X}).$$

- 5: Estimate $\tilde{F}_k(\mathbf{X}_k^{s,\ell})$ and $\tilde{F}_k(\mathbf{X}_k^0)$ by calling Algorithm 1 with $\Delta_k = \Delta_k^\ell$.
- 6: Compute the success ratio $\hat{\rho}_k$ as

$$\hat{\rho}_k^\ell = \frac{\tilde{F}_k(\mathbf{X}_k^0) - \tilde{F}_k(\mathbf{X}_k^{s,\ell})}{\max\{\zeta(\Delta_k^h)^2, M_k^\ell(\mathbf{X}_k^0) - M_k^\ell(\mathbf{X}_k^{s,\ell})\}}. \quad (15)$$

- 7: **if** $\hat{\rho}_k \geq \eta$ **then**
- 8: **return** $[\check{\mathbf{X}}_k^\ell = \mathbf{X}_k^{s,\ell}, I_k^h = \text{False}]$
- 9: **else**
- 10: **return** $[\check{\mathbf{X}}_k^\ell = \mathbf{X}_k^0, I_k^h = \text{True}]$
- 11: **end if**

function contributes to optimization within the current TR. At each iteration k , the algorithm checks if α_k exceeds a user-defined threshold $\alpha_{th} \in (0, 1)$. If so, it constructs M_k^ℓ using the LF design set \mathcal{X}_k^ℓ and corresponding estimates, then minimizes \mathcal{X}_k^ℓ within the TR $\mathcal{B}(\mathbf{X}_k; \Delta_k^\ell)$. If the candidate achieves a sufficient decrease in the HF function and has a sufficiently large model gradient norm, it is accepted, the TR expands, and α_k increases. Otherwise, the candidate is rejected, leading to the contraction of Δ_k^ℓ , a decrease in α_k , and progression to Step 1 in Algorithm 3 to identify a superior candidate within the shrunken TR. This process repeats until $\alpha_k < \alpha_{th}$, indicating that the LF oracle is no longer helpful. We note that the initial value α_0 should be chosen carefully, as poor initialization can slow early progress. However, its impact diminishes as the algorithm progresses, similar to the effect of an improperly chosen initial TR radius.

Remark 2. The sufficient reduction test for the LF model, involving $\hat{\rho}_k^\ell$, differs from the test involving $\hat{\rho}_k$ in Algorithm 2. Specifically, for a successful iteration, the reduction in function estimates must be larger than $\zeta(\Delta_k^h)^2$ for some $\zeta > 0$ (See Step 6 in Algorithm 3). This condition prevents the acceptance of a candidate solution based on an insignificant reduction in the local model value in (15), and is also reflected in the convergence analysis of ASTRO-BFDF.

When the LF-based search fails to identify the next iterate, the algorithm constructs the HF-based local model M_k^h . The design set \mathcal{X}_k is formed by reusing previously visited points whenever possible, including those from the LF-based models in the current iteration. HF function values are then estimated using BFAS, which also provides LF estimates. Then, we can additionally derive estimates for the LF function $\bar{F}^\ell(\mathbf{X}_k^i, T_k^i)$, aligning with the adaptive sampling rule (14), by obtaining $\max\{0, T_k^i - V_k^i\}$ more LF samples, which is typically small in practice and thus incurs

minimal computational burden. Both HF-based and LF-based local models are then constructed, their minimizers evaluated, and the better candidate is chosen as the next iterate. Finally, the TR radius Δ_k^h and the adaptive correlation constant are updated based on the sufficient reduction test.

In Algorithm 2, the LF-based local models are constructed at various points, each serving distinct purposes. Specifically, within Algorithm 3, the model is employed to seek an improved solution for the HF function. This decision stems from the belief that, when $\alpha_k > \alpha_{th}$, the LF model will provide sufficiently informative local approximations that can support the HF optimization. Thus, HF oracle usage is minimized. In the outer loop, the primary objective is to update the adaptive correlation constant, even in cases where the LF function has not proven beneficial in preceding iterations. In this case, our aim is to minimize reliance on the LF function, a goal achievable through the adoption of BFMC. When the HF function values are estimated at Step 15 in ASTRO-BFDF, a substantial number of LF samples are already available from BFMC, enabling the construction of M_k^ℓ at negligible additional cost. A drawback is that when the LF-based model fails to contribute meaningfully, Algorithm 2 may incur higher computational cost than HF-only solvers. This additional cost is an inherent trade-off for assessing the correlation, which is essential for determining its role in optimization. However, BFAS mitigates this overhead in practice by limiting unnecessary LF oracle evaluations.

4 Convergence Analysis

In this section, we present the convergence analysis of ASTRO-BFDF. We first introduce two additional assumptions concerning the local model. First, the minimizer of the local model is assumed to satisfy a certain degree of function reduction, known as the Cauchy reduction (See Definition 2). Second, the Hessian of the local model is assumed to be uniformly bounded. Both of these assumptions are essential to validate the quality of the candidate point generated at each iteration.

Assumption 3 (Reduction in Subproblem). *For some $\kappa_{fcd} \in (0, 1]$, $q \in \{h, \ell\}$, and all k , $M_k^q(\mathbf{X}_k^0) - M_k^q(\mathbf{X}_k^{s,q}) \geq \kappa_{fcd} (M_k^q(\mathbf{X}_k^0) - M_k^q(\mathbf{X}_k^0 + \mathbf{S}_k^c))$, where \mathbf{S}_k^c is the Cauchy step.*

Assumption 4 (Bounded Hessian in Norm). *In ASTRO-BFDF, the local model Hessians \mathbf{H}_k^q are bounded by $\kappa_{\mathbf{H}}^q$ for all k and $q \in \{h, \ell\}$ with $\kappa_{\mathbf{H}}^q \in (0, \infty)$ almost surely.*

4.1 Main Result

The convergence analysis of ASTRO-DF has received considerable attention in prior works such as [24, 35]. Although our analysis follows a similar framework, there are two crucial considerations we must address.

- (a) (Stochastic noise) BFMC must satisfy conditions analogous to those in Theorem 1, ensuring that the stochastic error in BFMC is less than $\mathcal{O}((\Delta_k^q)^2)$ for $q \in \{h, \ell\}$ after sufficiently large k . To achieve this, a crucial prerequisite (See Assumption 2) is ensuring that $F^h(\mathbf{x}, \xi^h) - cF^\ell(\mathbf{x}, \xi^\ell)$ exhibits similar properties to $F^h(\mathbf{x}, \xi^h)$ for any $\xi^h \in \Xi^h$, $c > 0$, and $\mathbf{x} \in \mathbb{R}^d$.
- (b) (Trust-region) The TR sizes for both HF and LF functions need to converge to zero. Similar to other stochastic TR methods [24, 31, 41], this condition is essential because function estimation errors are bounded, even in the worst-case, on the order of $\mathcal{O}(\Delta_k^p)$ for some $p > 0$ under specific sampling rules and assumptions. Consequently, the estimation errors

will also converge to zero, ensuring the accuracy of the estimates. Therefore, within BFSO, we also need the same result for Δ_k^h . Furthermore, since $\Delta_k^h \geq \Delta_k^\ell$ for all $k \in \mathbb{N}$, the convergence of Δ_k^h implies the convergence of Δ_k^ℓ as well.

Taking into account the aforementioned considerations, we are now poised to present the convergence theory of ASTRO-BFDF.

Theorem 2 (Almost Sure Convergence). *Let Assumptions 1-4 hold. Then,*

$$\lim_{k \rightarrow \infty} \|\nabla f^h(\mathbf{X}_k)\| \xrightarrow{w.p.1} 0. \quad (16)$$

Theorem 2 guarantees that a sequence $\{\mathbf{X}_k(\omega)\}$ generated by Algorithm 2 converges to the first-order stationary point for any solution sample path ω .

4.2 Proof of Theorem 2

We start by demonstrating that the iid random variables $E_{k,j}^{i,h} - cE_{k,j}^{i,l}$ also fulfill Assumption 2 for any $k \in \mathbb{N}$, $c \in \mathfrak{R}$, and $i \in \{0, 1, 2, \dots, p, s\}$, indicating their adherence to a sub-exponential distribution.

Lemma 5. *Let Assumption 2 holds. Then there exist $\sigma^2 > 0$ and $b > 0$ such that for a fixed n and $c \in \mathfrak{R}$,*

$$\frac{1}{n} \sum_{j=1}^n \mathbb{E}[|E_{k,j}^{i,h} - cE_{k,j}^{i,l}|^m \mid \mathcal{F}_{k,j-1}] \leq \frac{m!}{2} b^{m-2} \sigma^2, \quad \forall m = 2, 3, \dots, \forall k. \quad (17)$$

Proof. Let us first arbitrary choose σ^h , σ^ℓ , b^h , and b^ℓ such that $\sigma^h > \sigma^\ell > 0$, $b^h > b^\ell$, and Assumption 2 holds. We obtain from the Minkowski inequality and Assumption 2 that for any $k, j \in \mathbb{N}$, $c \in \mathfrak{R}$, and any $m \in \{2, 3, \dots\}$, there exist $b^h, b^\ell, (\sigma^h)^2, (\sigma^\ell)^2 > 0$ such that

$$\begin{aligned} \mathbb{E}[|E_{k,j}^{i,h} - cE_{k,j}^{i,l}|^m \mid \mathcal{F}_{k,j-1}] &\leq \left(\mathbb{E}[|E_{k,j}^{i,h}|^m \mid \mathcal{F}_{k,j-1}]^{\frac{1}{m}} + \mathbb{E}[|cE_{k,j}^{i,l}|^m \mid \mathcal{F}_{k,j-1}]^{\frac{1}{m}} \right)^m \\ &\leq \left(\left(\frac{m!}{2} (b^h)^{m-2} (\sigma^h)^2 \right)^{\frac{1}{m}} + c \left(\frac{m!}{2} (b^\ell)^{m-2} (\sigma^\ell)^2 \right)^{\frac{1}{m}} \right)^m. \end{aligned} \quad (18)$$

Then there must exist some constant $\alpha_\sigma, \alpha_b > 1$ such that $\alpha_\sigma (\sigma^\ell)^2 = (\sigma^h)^2$ and $\alpha_b b^\ell = b^h$. Then the right-hand side of (18) becomes $((\alpha_\sigma^2 \alpha_b^{m-2})^{1/m} + c)^m (2^{-1} m! (b^\ell)^{m-2} (\sigma^\ell)^2)$. Since $(\alpha_\sigma^2 \alpha_b^{m-2})^{1/m} \leq \alpha_\sigma \alpha_b$ for all $m \in \{2, 3, \dots\}$, we obtain

$$\frac{1}{n} \sum_{j=1}^n \mathbb{E}[|E_{k,j}^{i,h} - cE_{k,j}^{i,l}|^m \mid \mathcal{F}_{k,j-1}] \leq \frac{m!}{2} ((\alpha_\sigma \alpha_b + c) b^\ell)^{m-2} ((\alpha_\sigma \alpha_b + c) \sigma^\ell)^2.$$

Hence, the statement of the theorem holds with $\sigma = \sigma^\ell (\alpha_\sigma \alpha_b + c)$ and $b = (\alpha_\sigma \alpha_b + c) b^\ell$. If $\sigma^h \leq \sigma^\ell$ or $b^h \leq b^\ell$, we set $\check{\sigma}^h = 2\sigma^\ell$ and $\check{b}^h = 2b^\ell$. With this choice, (7) continues to hold with $\check{\sigma}^h$ and \check{b}^h in place of σ^h and b^h , and the proof follows from the same steps as above. \square

Now let us prove that the function estimate error from BFAS is bounded by $\mathcal{O}((\Delta_k^q)^2)$ with probability one after sufficiently large k , aligning with the outcome stated in Theorem 1.

Lemma 6. *Let Assumption 2 holds and \mathbf{X}_k^i for $i \in \{0, 1, 2, \dots, p, s\}$ be the design points generated by Algorithm 2 at iteration k . Let $\tilde{F}(\mathbf{X}_k^i) = f(\mathbf{X}_k^i) + \tilde{E}_k^i$ be the HF function estimate obtained from Algorithm 1 with $\Delta_k = \Delta_k^q$ for $q \in \{h, \ell\}$. Then, given $c_f > 0$,*

$$\mathbb{P}\{|\tilde{E}_k^i| \geq c_f(\Delta_k^q)^2 \text{ i.o.}\} = 0. \quad (19)$$

Proof. Let $\omega \in \Omega$. Firstly, if the function estimate from BFAS was obtained by CMC, we know from Theorem 1 and Borel-Cantelli's first lemma for martingales [37] that the statement of the lemma is satisfied. Now, we assume that the function estimate $\tilde{F}(\mathbf{X}_k^i(\omega))$ is obtained using BFMC, implying that

$$|\tilde{E}_k^i(\omega)| = |\bar{E}_k^{i,h}(N_k^i(\omega)) - C_k(\omega)\bar{E}_k^{i,l}(N_k^i(\omega)) + C_k(\omega)\bar{E}_k^{i,l}(V_k^i(\omega))|,$$

where $\bar{E}_k^{i,q}(N_k^i(\omega)) = N(\mathbf{X}_k^i(\omega))^{-1} \sum_{j=1}^{N(\mathbf{X}_k^i(\omega))} E_{k,j}^{i,q}(\omega)$ for $q \in \{h, \ell\}$, $N_k^i(\omega) = N(\mathbf{X}_k^i(\omega))$, and $V_k^i(\omega) = V(\mathbf{X}_k^i(\omega))$. To simplify notation, we will omit ω from this point forward. Then we have

$$\begin{aligned} \mathbb{P}\{|\tilde{E}_k^i| \geq c_f(\Delta_k^q)^2 | C_k = c\} &\leq \mathbb{P}\{|\bar{E}_k^{i,h}(N_k^i) - c\bar{E}_k^{i,l}(N_k^i)| \geq \frac{c_f}{2}(\Delta_k^q)^2 | C_k = c\} \\ &\quad + \mathbb{P}\{|c\bar{E}_k^{i,l}(V_k^i)| \geq \frac{c_f}{2}(\Delta_k^q)^2 | C_k = c\}. \end{aligned} \quad (20)$$

We know from Step 1 in Algorithm 1 that N_k^i and V_k^i are greater than or equal to $\sigma_0^2 \lambda_k \kappa^{-2} (\Delta_k^q)^{-4}$. We also know from Lemma 5 that Assumption 2 holds for $E_{k,0}^{i,h} - cE_{k,0}^{i,l}$, implying that Theorem 1 also applies to $E_{k,j}^{i,h} - cE_{k,j}^{i,l}$ for any $j \in \mathbb{N}$. Hence, the right-hand side of (20) is summable, from which we obtain $\mathbb{P}\{|\tilde{E}_k^i| \geq c_f(\Delta_k^q)^2\}$ is also summable based on $\mathbb{P}\{|\tilde{E}_k^i| \geq c_f(\Delta_k^q)^2\} = \mathbb{E}[\mathbb{P}\{|\tilde{E}_k^i| \geq c_f(\Delta_k^q)^2 | C_k = c\}]$. As a result, the statement of the theorem holds with Borel-Cantelli's first lemma for martingales [37].

□

Next, we demonstrate that as k goes to infinity, both TR radii converge to zero almost surely. Despite the main framework of our proof differing trivially from the one presented in [41], we opt to provide a comprehensive proof to facilitate understanding in Appendix B.

Lemma 7. *Let Assumptions 1-4 hold. Then,*

$$\Delta_k^h \xrightarrow{w.p.1} 0 \text{ and } \Delta_k^\ell \xrightarrow{w.p.1} 0 \text{ as } k \rightarrow \infty.$$

Proof. See Appendix B. □

Relying on Lemma 7, we show through Lemma 8 that the gradient of the model for the HF function converges to the true gradient almost surely. It is worth highlighting that the local model for the HF function is not constructed at every iteration, as sometimes the local model for the LF function can discover a better solution.

Lemma 8. *Let Assumptions 1-4 hold. Let $\{k_j\}$ be the subsequence such that $I_{k_j}^h = \text{True}$. Then,*

$$\|\nabla M_{k_j}^h(\mathbf{X}_{k_j}^0) - \nabla f^h(\mathbf{X}_{k_j}^0)\| \xrightarrow{w.p.1} 0 \text{ as } j \rightarrow \infty.$$

Proof. We know from Lemma 6 that given $c_f > 0$, there exists sufficiently large J such that $|\tilde{E}_{k_j}^i| < c_f(\Delta_{k_j}^h)^2$ for any $i \in \{0, 1, \dots, p, s\}$ and $j > J$. Then from Lemma 2, we have,

$$\begin{aligned} \|\nabla M_{k_j}^h(\mathbf{X}_{k_j}^0) - \nabla f^h(\mathbf{X}_{k_j}^0)\| &\leq \kappa_{eg1}\Delta_{k_j}^h + \kappa_{eg2}\frac{\sqrt{\sum_{i=1}^p(\tilde{E}_{k_j}^i - \tilde{E}_{k_j}^0)^2}}{\Delta_{k_j}^h} \\ &\leq \kappa_{eg1}\Delta_{k_j}^h + \kappa_{eg2}\frac{\sum_{i=1}^p|\tilde{E}_{k_j}^i - \tilde{E}_{k_j}^0|}{\Delta_{k_j}^h} \\ &\leq (\kappa_{eg1} + 2p\kappa_{eg2}c_f)\Delta_{k_j}^h. \end{aligned} \quad (21)$$

Given that Lemma 7 ensures $\Delta_{k_j}^h$ converges to 0 w.p.1, the statement of the theorem holds. \square

In the following lemma, we demonstrate that after a sufficient number of iterations, if the TR for the HF function is relatively smaller than the model gradient norm, the iteration is successful with probability one.

Lemma 9. *Let Assumptions 1-4 hold. Then there exists $c_d > 0$ such that*

$$\mathbb{P}\left\{\left(\Delta_k^h \leq c_d\|\nabla M_k^h(\mathbf{X}_k^0)\|\right) \cap (\hat{\rho}_k < \eta) \cap \left(I_k^h \text{ is True}\right) \text{ i.o.}\right\} = 0.$$

Proof. See Appendix C. \square

Given Lemma 8 and 9, next result suggests that if the TR radius for the HF function is comparatively smaller than the true gradient norm, the candidate solution is accepted and the TR is expanded. This ensures that the TR for the HF function will not converge to zero before the true gradient does.

Lemma 10. *Let Assumptions 1-4 hold. Then there exists a constant $c_{lb} > 0$ such that with probability 1*

$$\Delta_k^h < c_{lb}\|\nabla f^h(\mathbf{X}_k^0)\| \text{ for sufficiently large } k \Rightarrow \text{Iteration } k \text{ is successful.}$$

Proof. Let the solver sample path ω be fixed. When I_k^h is False, the iteration k is already successful. Hence, let us assume $I_k^h = \text{True}$, implying that the local model M_k^h must exist. We know from (21) that for sufficiently large k , $\|\nabla M_k^h(\mathbf{X}_k^0) - \nabla f^h(\mathbf{X}_k^0)\| \leq c_{gd}\Delta_k^h$, where $c_{gd} = \kappa_{eg1} + 2p\kappa_{eg2}c_f$. Define $c_{lb} = \frac{\min\{c_d, \mu\}}{1 + \min\{c_d, \mu\}c_{gd}}$, where c_d is as defined in Lemma 9. Then we have

$$\Delta_k^h \leq c_{lb}\|\nabla f^h(\mathbf{X}_k^0)\| \leq c_{lb}(\|\nabla M_k^h(\mathbf{X}_k^0)\| + \|\nabla f^h(\mathbf{X}_k^0) - \nabla M_k^h(\mathbf{X}_k^0)\|), \quad (22)$$

from which we obtain

$$\Delta_k^h \leq \frac{c_{lb}}{1 - c_{lb}c_{gd}}\|\nabla M_k^h(\mathbf{X}_k^0)\| = \min\{c_d, \mu\}\|\nabla M_k^h(\mathbf{X}_k^0)\|. \quad (23)$$

We also know from Lemma 9 that when $\Delta_k^h \leq c_d\|\nabla M_k^h(\mathbf{X}_k^0)\|$, $\hat{\rho}_k \geq \eta$ for sufficiently large k . As a result, when $\Delta_k^h \leq c_{lb}\|\nabla f^h(\mathbf{X}_k^0)\|$, we have $\Delta_k^h \leq \mu\|\nabla M_k^h(\mathbf{X}_k^0)\|$ and $\hat{\rho}_k \geq \eta$ for sufficiently large k , implying that the iteration k is successful. \square

Lemma 11. *Let Assumptions 1-4 hold. Then*

$$\liminf \|\nabla f^h(\mathbf{X}_k)\| \xrightarrow{w.p.1} 0 \text{ as } k \rightarrow \infty. \quad (24)$$

Proof. We begin by noting that when I_k^h is False, iteration k must be successful. Using this fact, along with Lemma 8 and 9, the proof can be completed by straightforwardly following the steps outlined in Theorem 4.6 of [41]. \square

We have reached a point where we can establish the almost sure convergence of ASTRO-BFDF. The proof follows a similar approach to that of the classical TR method. For further details, see [24, 33, 42]. We now prove Theorem 2.

Proof. of Theorem 2. We first need to assume that there is a subsequence that has gradients bounded away from zero for contradiction. Particularly, suppose that there exists a set, $\hat{\mathcal{D}}$, of positive measure, $\omega \in \hat{\mathcal{D}}$, $\epsilon_0 > 0$, and a subsequence of successful iterates, $\{t_j(\omega)\}$, such that $\|\nabla f^h(\mathbf{X}_{t_j(\omega)}(\omega))\| > 2\epsilon_0$, for all $j \in \mathbb{N}$. We denote $t_j = t_j(\omega)$ and suppress ω in the following statements for ease of notation. Due to the lim-inf type of convergence just proved in Lemma 11, for each t_j , there exists a first successful iteration, $\ell_j = \ell(t_j) > t_j$, such that, for large enough k ,

$$\|\nabla f^h(\mathbf{X}_k)\| > 2\epsilon_0, \quad t_j \leq k < \ell_j, \quad (25)$$

and

$$\|\nabla f^h(\mathbf{X}_{\ell_j})\| < 1.5\epsilon_0. \quad (26)$$

Define $\mathcal{A}_j^h = \{k \in \mathcal{H} : t_j \leq k < \ell_j\}$ and $\mathcal{A}_j^\ell = \{k \in \mathcal{L} : t_j \leq k < \ell_j\}$, where

$$\begin{aligned} \mathcal{H} &= \{k \in \mathbb{N} : (\hat{\rho}_k > \eta) \cap (\mu \|\nabla M_k^h(\mathbf{X}_k^0)\| \geq \Delta_k^h) \cap (I_k^h \text{ is True})\}, \\ \mathcal{L} &= \{k \in \mathbb{N} : I_k^h \text{ is False}\}. \end{aligned}$$

Let j be sufficiently large and $k \in \mathcal{A}_j^h$. We then obtain from Lemma 8

$$\|\nabla M_k^h(\mathbf{X}_k)\| > \epsilon_0. \quad (27)$$

Since k is a successful iteration, $\hat{\rho}_k \geq \eta$. Furthermore, Assumption 3 and (27) imply that

$$\begin{aligned} f^h(\mathbf{X}_k) - f^h(\mathbf{X}_{k+1}) + \tilde{E}_k^0 - \tilde{E}_k^s &\geq \frac{1}{2} \eta \kappa_{fcd} \|\nabla M_k^h(\mathbf{X}_k)\| \min \left\{ \frac{\|\nabla M_k^h(\mathbf{X}_k)\|}{\|\mathbf{H}_k^h\|}, \Delta_k^h \right\} \\ &> c_{fd} \Delta_k^h, \end{aligned} \quad (28)$$

where $c_{fd} = \min\{\frac{1}{2}\eta\kappa_{fcd}, 2\zeta\gamma_2 c_{lb}\}\epsilon_0$. When $k \in \mathcal{A}_j^\ell$, we also obtain

$$\begin{aligned} f^h(\mathbf{X}_k) - f^h(\mathbf{X}_{k+1}) + \tilde{E}_k^0 - \tilde{E}_k^s &> \zeta(\Delta_k^h)^2 > \zeta\gamma_2 c_{lb} \|\nabla f(\mathbf{X}_k)\| \Delta_k^h \\ &> 2\zeta\gamma_2 c_{lb} \epsilon_0 \Delta_k^h \geq c_{fd} \Delta_k^h, \end{aligned} \quad (29)$$

where the second inequality is obtained from Lemma 10, implying that $\Delta_k^h > \gamma_2 c_{lb} \|\nabla f(\mathbf{X}_k)\|$ for sufficiently large k and the third inequality follows from $\|f(\mathbf{X}_k)\| > 2\epsilon_0$. Since we know from Lemma 6 that

$$|\tilde{E}_k^0 - \tilde{E}_k^s| < 0.5c_{fd}\Delta_k^h \text{ for } k \in \mathcal{A}_j^h \text{ and } |\tilde{E}_k^0 - \tilde{E}_k^s| < 0.5c_{fd}\Delta_k^\ell \text{ for } k \in \mathcal{A}_j^\ell, \quad (30)$$

the sequence $\{f^h(\mathbf{X}_k)\}_{k \in \mathcal{A}_j}$ is monotone decreasing for sufficiently large j . From (29), (30), and the fact that the step size cannot exceed the TR radius, we deduce that

$$\begin{aligned} \|\mathbf{X}_{t_j} - \mathbf{X}_{\ell_j}\| &\leq \sum_{i \in \mathcal{A}_j} \|\mathbf{X}_i - \mathbf{X}_{i+1}\| \leq \sum_{i \in \mathcal{A}_j^h} \Delta_i^h + \sum_{i \in \mathcal{A}_j^\ell} \Delta_i^\ell \\ &\leq \frac{2(f^h(\mathbf{X}_{t_j}) - f^h(\mathbf{X}_{\ell_j}))}{c_{fd}}. \end{aligned} \quad (31)$$

Now define $\mathcal{B}_j = \{k \in \mathcal{K} : \ell_j \leq k < t_{j+1}\}$, where $\mathcal{K} = \mathcal{H} \cup \mathcal{L}$. Let $k \in \mathcal{B}_j$ for sufficiently large j . From Lemma 6, (33), (34), and the fact that $\Delta_k^h > \Delta_k^\ell$ for any $k \in \mathbb{N}$, we obtain $f^h(\mathbf{X}_k) - f^h(\mathbf{X}_{k+1}) \geq 0.5\kappa_R(\Delta_k^\ell)^2$, implying that the sequence $\{f^h(\mathbf{X}_k)\}_{k \in \mathcal{A}_j \cup \mathcal{B}_j}$ is monotone decreasing for sufficiently large j . The boundedness of f^h from below then implies that the right-hand side of (31) converges to 0 as j goes to infinity, concluding that $\lim_{j \rightarrow \infty} \|\mathbf{X}_{t_j} - \mathbf{X}_{\ell_j}\| = 0$. Consequently, by continuity of the gradient, we obtain that $\lim_{j \rightarrow \infty} \|\nabla f^h(\mathbf{X}_{t_j}) - \nabla f^h(\mathbf{X}_{\ell_j})\| = 0$. However, this contradicts $\|\nabla f^h(\mathbf{X}_{t_j}) - \nabla f^h(\mathbf{X}_{\ell_j})\| > 0.5\epsilon_0$, obtained from (25) and (26). Thus, (16) must hold. \square

5 Numerical Experiments

We will now assess and compare ASTRO-BFDF with other simulation optimization solvers. The experiments consider two categories of test problems: synthetic problems and problems with discrete event simulation (DES).

Synthetic problems constitute deterministic problems with artificial Gaussian noise. Since the analytical form of f^h is known, generating numerous problems that adhere to predetermined assumptions becomes relatively straightforward. However, since both the function f^h and the stochastic noises are artificially generated, the performance of the solvers on these problems may not reflect solver effectiveness on real-world problems. In particular, when the same random number stream is used, the stochastic noises at different design points will be identical, implying that $F^h(\cdot, \xi^h) - f^h(\cdot)$ is a constant function given fixed $\xi^h \in \Xi^h$. This setting satisfies a stricter assumption than the one posed in this paper. To provide more realistic testing, we also evaluated the solvers on problems involving DES, which mimics real-world conditions and generates multiple outputs utilized within the objective function. All experiments have been implemented using SimOpt [43].

We evaluate the performance of each algorithm through a two-stage experimental design. In the first stage, each solver is tested on every problem instance through 20 independent optimization runs under a problem-specific simulation budget. This budget governs all aspects of the solver's decision-making process, such as where to evaluate and how many times to sample. In the bi-fidelity setting, simulation costs vary by fidelity level; we assign a unit cost to HF evaluations (i.e., $w^h = 1$), while LF evaluations incur a fractional cost (e.g., $w^\ell = 0.5$). For example, querying the HF model 10 times and the LF model 20 times would consume $10 \times w^h + 20 \times w^\ell = 20$ units of budget. The reported budget accounts only for simulation costs; computational overhead, such as solving TR subproblems or updating surrogate models in BO, is excluded, as the problem setup (outlined in Section 1) assumes simulations to be the dominant computational cost. In the second stage, after obtaining the solution sequences $\{\mathbf{X}_k\}$ from all runs, each visited solution is evaluated using 200 HF replications. These evaluations provide unbiased objective estimates and ensure fair comparisons across solvers.

We compare ASTRO-BFDF with ASTRO-DF, Bi-fidelity Bayesian Optimization (BFBO) [9], Bi-fidelity sample average gradient (BFSAG) [44], and ADAM [45]. Details of the implementation as well as hyperparameter tuning can be found in Appendix D. In implementing the solvers, we applied CRN, which involves using the same random input ω_i to reduce the variance of BFMC-based function estimates and the estimated function reductions between design points. That is, both HF and LF evaluations use correlated inputs $\xi^h(\omega_i)$ and $\xi^\ell(\omega_i)$, and the same random input ω_i is also shared across different design points. To integrate CRN into ASTRO-BFDF, each time a local model is constructed, the sample sizes and the coefficient at the center point, obtained through BFAS, are preserved and subsequently utilized for estimating the function values at other design points. Although incorporating CRN often requires custom coding, SimOpt provides standardized interfaces that make integration straightforward. Without such infrastructure, implementing CRN and adaptive strategies would involve significant solver-specific effort, indicating a critical dependency of the numerical experiments on SimOpt.

5.1 Synthetic Problems

We consider four deterministic HF functions f^h and construct LF counterparts based on a correlation parameter κ_{cor} . The LF function $f^\ell(\mathbf{x}, \kappa_{cor})$ may closely resemble or differ significantly from $f^h(\mathbf{x})$ depending on κ_{cor} . Details of these functions are provided in Appendix E. We have tested the problems with three different values of κ_{cor} : 0.1, 0.5, and 0.9. Regarding the stochastic noises, a more complex setup is required to determine whether BFAS can enhance computational efficiency. For instance, test problems should include an instance with a high variance of the LF oracle, which can make BFMC undesirable during the optimization. Thus, we examined the configuration in which the stochastic noises for the HF and LF oracles follow $\mathcal{N}(0, c_{sd} + 0.05X_k[0])$ with $c_{sd}^h \in \{5, 10, 15\}$, where $X_k[0]$ denotes the first coordinate of the current solution \mathbf{X}_k . The additional term $0.05x[0]$ ensures that noise terms vary across design points under CRN. Combining four HF functions, three LF configurations, and three noise settings for each fidelity yields a total of $4 \times 3 \times 3 = 108$ synthetic test problems.

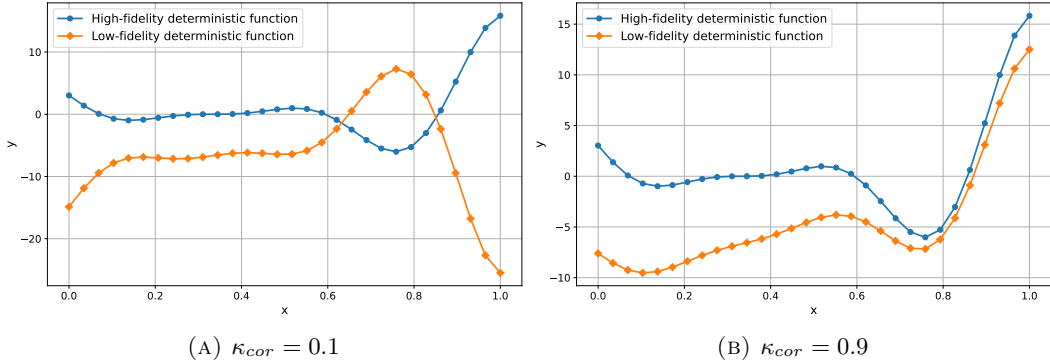


FIGURE 2: Loss landscapes of Forrester functions with varying κ_{cor} .

We begin by presenting numerical results on synthetic problems with varying κ_{cor} . Although κ_{cor} does not directly represent linear similarity between f^h and f^ℓ , it induces significant changes in LF function behaviors (see Figure 2). When $\kappa_{cor} = 0.9$, the LF function provides useful information—such as the sign of the gradient—that supports HF optimization, whereas for $\kappa_{cor} = 0.1$, it provides minimal benefit. To assess the impact of κ_{cor} on solver performance, we first tested ASTRO-BFDF, ASTRO-DF, and BFBO on the Forrester functions shown in Figure 2,

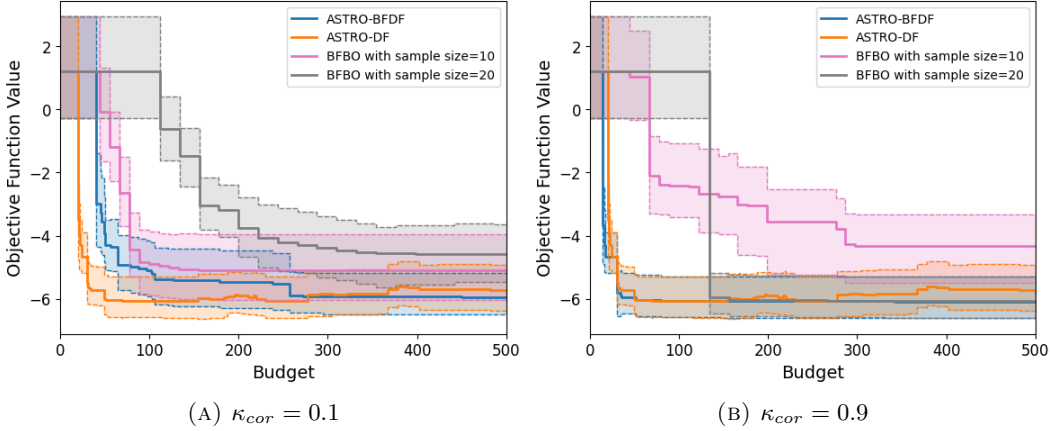


FIGURE 3: Finite-time performance on Forretal functions with cost ratio 1:0.1, $c_{sd}^h = c_s d^\ell = 15$, and (a) $\kappa_{cor} = 0.1$ and (b) $\kappa_{cor} = 0.9$.

augmented with stochastic noise. See Figure 3. ASTRO-BFDF reaches near-optimal solutions faster when $\kappa_{cor} = 0.9$ compared to $\kappa_{cor} = 0.1$. Notably, ASTRO-DF converges faster than ASTRO-BFDF when $\kappa_{cor} = 0.1$, but it often accepts suboptimal solutions because of stochastic noise. In contrast, ASTRO-BFDF ultimately attains better solutions by leveraging BFMC for variance reduction in function estimates. BFBO with a sample size of 20 fails to reach the optimum when $\kappa_{cor} = 0.1$. These results indicate that BFBO is effective only under strong correlation, as discussed in Section 1. Lastly, when the sample size is reduced to 10 in BFBO, the function estimates are not sufficiently accurate, preventing it from achieving the optimal solution in either case. This further shows that BFBO requires highly accurate function estimates to effectively solve stochastic optimization problems, which makes it inefficient and challenging to determine appropriate sample sizes.

We now compare solver performance across all 108 synthetic problems using solvability profiles, a standard tool for evaluating solver effectiveness in simulation optimization. Each curve in a profile represents the fraction of problems that a solver successfully solves within a specified relative optimality gap. For example, ADAM solves about 20% of the problems to within a 1% optimality gap after using 30% of the budget allocated to each problem in Figure 4a. The optimality gap is calculated based on the best solution found among all tested solvers, even when the true optimum is known, to mimic practical conditions and allow fair comparisons.

In Figure 4, when the cost ratio of calling HF and LF oracles stands at 1:0.1, ASTRO-BFDF emerges as a standout performer, solving over 60% of the problems within a mere 20% of the budget. Even when LF evaluations cost the same as HF evaluations (1:1), ASTRO-BFDF finds better solutions than ASTRO-DF (see Figure 4b). This suggests that utilizing the LF function could be beneficial for optimization, even when its computational cost is comparable to that of the HF function. Hence, we will next delve deeper into the specific scenarios where leveraging the LF function proves advantageous for optimization.

Previous studies [39, 40] often use the correlation between LF and HF functions (or between LF and a surrogate model) to determine whether LF evaluations should be employed. However, even though the LF function may exhibit a high correlation with the HF function in specific feasible regions, its usefulness can vary based on the optimization trajectory, such as the

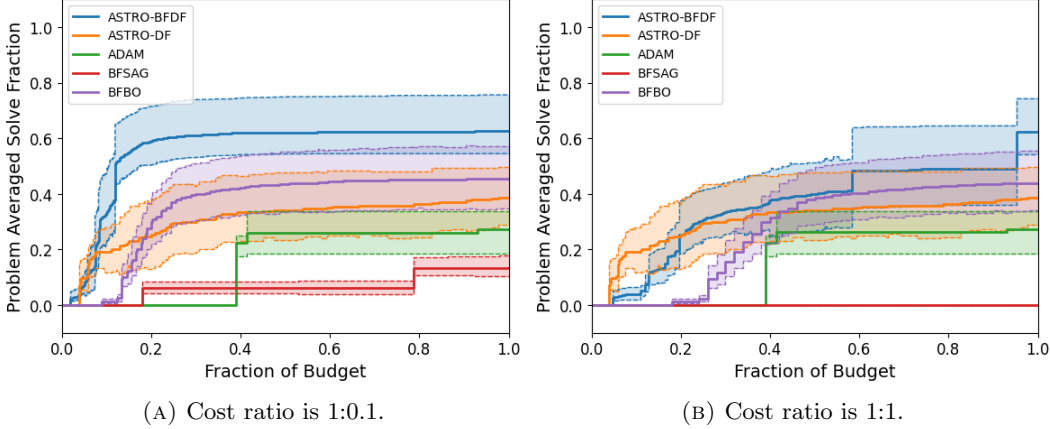


FIGURE 4: Fraction of 108 synthetic problems solved to within a 1% relative optimality gap (i.e., 0.01-optimality), with 95% confidence intervals from 20 runs of each algorithm. In (a) and (b), the cost ratios are 1:0.1 and 1:1, respectively.

initial design point. Hence, correlation alone might not be a reliable indicator of LF usefulness. Instead of requiring strong global correlation, it is often sufficient to obtain an accurate gradient approximation at the current iterate. By incorporating an adaptive correlation constant and BFAS for variance reduction, ASTRO-BFDF achieves more accurate gradients and outperforms other solvers, even when there is significant bias between f^h and f^ℓ . To confirm this numerically, we now present results for problems where only the correlation constant κ_{cor} varies.

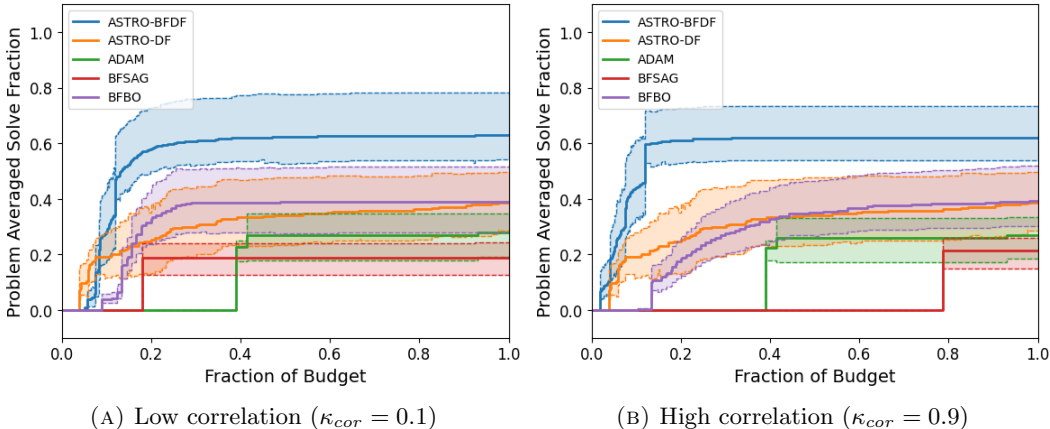


FIGURE 5: Solvability profiles of 36 problems measured at a 0.01 optimality gap, with 95% confidence intervals from 20 runs of each algorithm, under two different correlation settings between the LF and HF functions.

In Figure 5, ASTRO-BFDF consistently demonstrates superiority regardless of the correlation between the HF and LF functions. When the correlation is low (see Figure 5a), ASTRO-BFDF initially converges more slowly than ASTRO-DF during the first 10% of the budget, as it evaluates whether M_k^ℓ provides useful information. Once it prioritizes M_k^h , ASTRO-BFDF converges more rapidly to better solutions, benefiting from more accurate gradient approximations enabled by

BFAS, compared to ASTRO-DF.

The usefulness of the LF function in providing accurate gradient estimates can be maximized when it possesses unique structural properties, such as convexity, which may guide the search toward the global optimum of the non-convex HF function. In this case, BF optimization remains advantageous even when the LF oracle has high variance and cost. However, the opposite scenario is also possible, where the optimum of the LF function is located near a local optimum of the HF function, which may hinder progress.

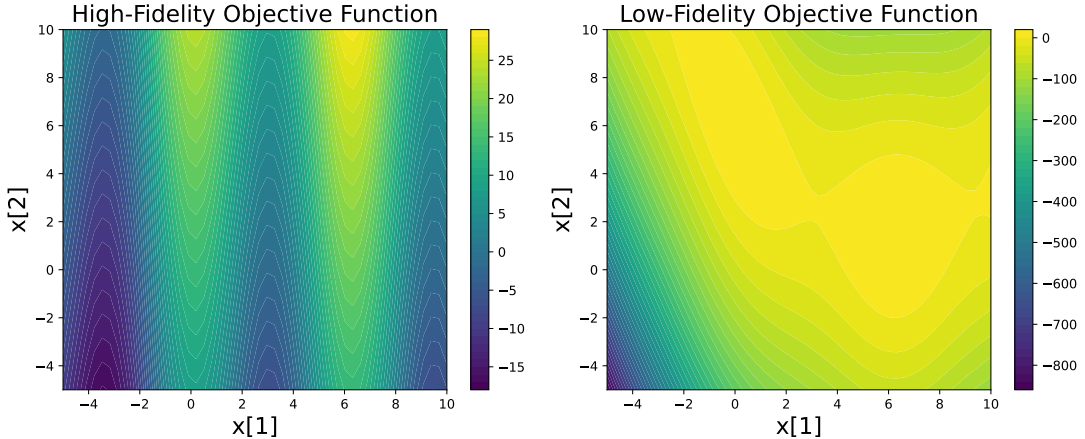


FIGURE 6: The contour maps of the HF and LF function without stochastic noises of the BRANIN problem with $\kappa_{cor} = 0$.

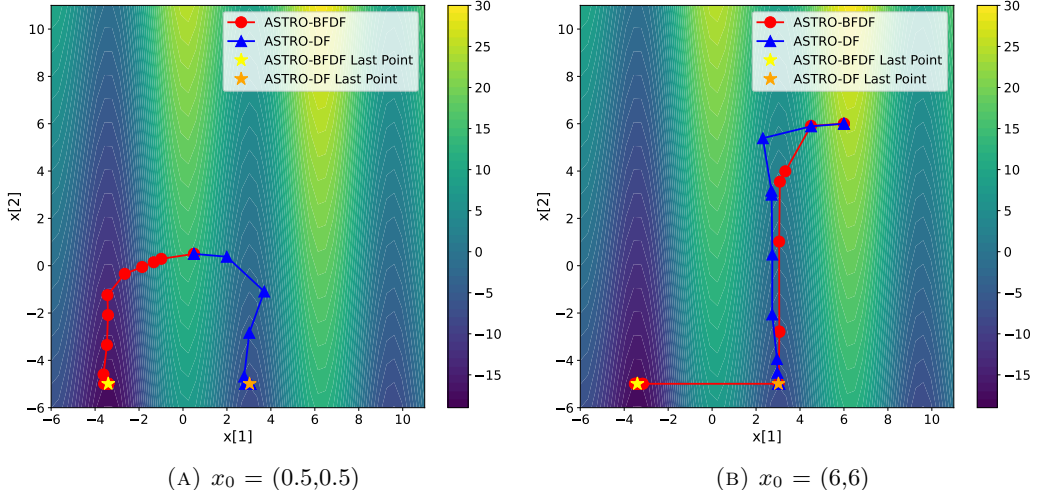


FIGURE 7: One sample path of $\{X_k\}$ with ASTRO-DF and ASTRO-BFDF on Branin function with $\kappa_{cor} = 0$ and a budget of 1000 HF oracle calls.

The Branin function is an example for which BF optimization can be highly effective due to the structure of the LF function. In Figure 6, the LF function possesses a favorable structure, which aligns with the global optimum of the HF function. Consequently, although directly finding the global optimum of the HF function is challenging due to its non-convexity, the solver can

leverage the LF function to guide the search toward the region near the global optimum. See Figure 7. Since the HF function is non-convex, ASTRO-DF often converges to a local optimum. In contrast, ASTRO-BFDF leverages the LF function and guides $\{\mathbf{X}_k\}$ toward the global optimum. Notably, even if $\{\mathbf{X}_k\}$ initially approaches to a local optimum, ASTRO-BFDF can escape by using locally convex structure of the LF function and ultimately reach the global optimum (see Figure 7b).

5.2 Problems with DES

In this section, we test more realistic problems using DES for the HF and LF simulation oracles. Specifically, we consider two problems: an M/M/1 queue problem and an inventory problem. In both cases, the DES model operates until a defined end time, denoted by T , thereby enabling the acquisition of BF results through variations in T . A simulation model with a longer end time is typically considered an HF model, as longer runs tend to produce more accurate estimates of the simulation output. For example, consider the case where the objective is to minimize inventory costs over 100 days. The HF model simulates the entire 100-day inventory system, capturing long-term dynamics and providing more accurate estimates of cumulative costs. In contrast, the LF simulation model runs over a shorter horizon, such as 30 days, which reduces computational time but may yield less precise estimates of steady-state performance. In this setting, the cost ratio between the HF and LF models stands at 1 : 0.3. A notable feature of this problem is that running one replication of the HF model inherently produces one replication of the LF model without incurring additional computational expenses.

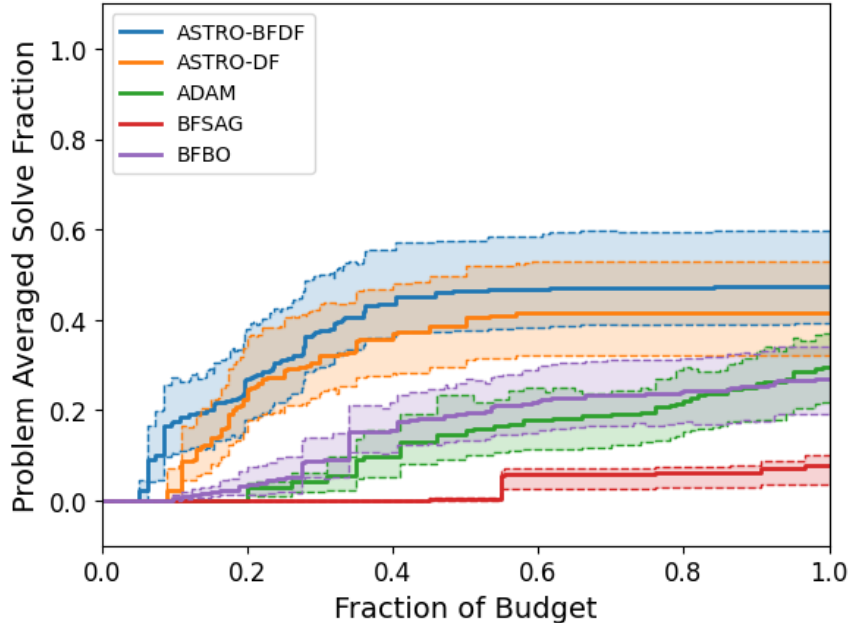


FIGURE 8: Solvability profiles of 25 problems with DES measured at a 0.01 optimality gap, with 95% confidence intervals from 20 runs of each algorithm.

Before delving into the details of each problem, we present the solvability profile for 25 instances (See Figure 8), including 5 instances from the M/M/1 problem and 20 instances from the inventory problem. The cost ratio between the HF and LF models for both problems is 1 : 0.3, indicating that the LF oracle simulates the system for $0.3T$ days. ASTRO-BFDF demonstrates

not only a faster convergence but also an enhanced ability to identify superior solutions by the end of the allocated budget.

5.2.1 M/M/1 Queue Problem

We employ a model that simulates an M/M/1 queue, characterized by exponential distributions for both inter-arrival and service times. Let λ and μ denote the rate parameters for interarrival and service times, respectively. The HF M/M/1 queue model simulates 100 random arrivals into the system, generating inter-arrival and service times for each customer. Based on these stochastic realizations, it estimates the average sojourn time for each arrival, representing the time a customer spends in the system from entry to departure under a given configuration. The randomness in the arrival and service processes is captured by ξ^h ; therefore, employing CRN implies generating the same sequence of arrivals and service times across different system configurations. The HF function is defined as $F^h(\mu, \xi^h) = 100^{-1} \sum_{i=1}^{100} s_i(\mu, \xi^h) + 0.1\mu^2$, where $s_i(\mu, \xi^h)$ denotes the sojourn time of the i -th customer, and the term $0.1\mu^2$ represents a penalty interpreted as an investment to increase the service rate μ . Therefore, the objective is to minimize the expected average sojourn time and a penalty, where μ acts as the decision variable.

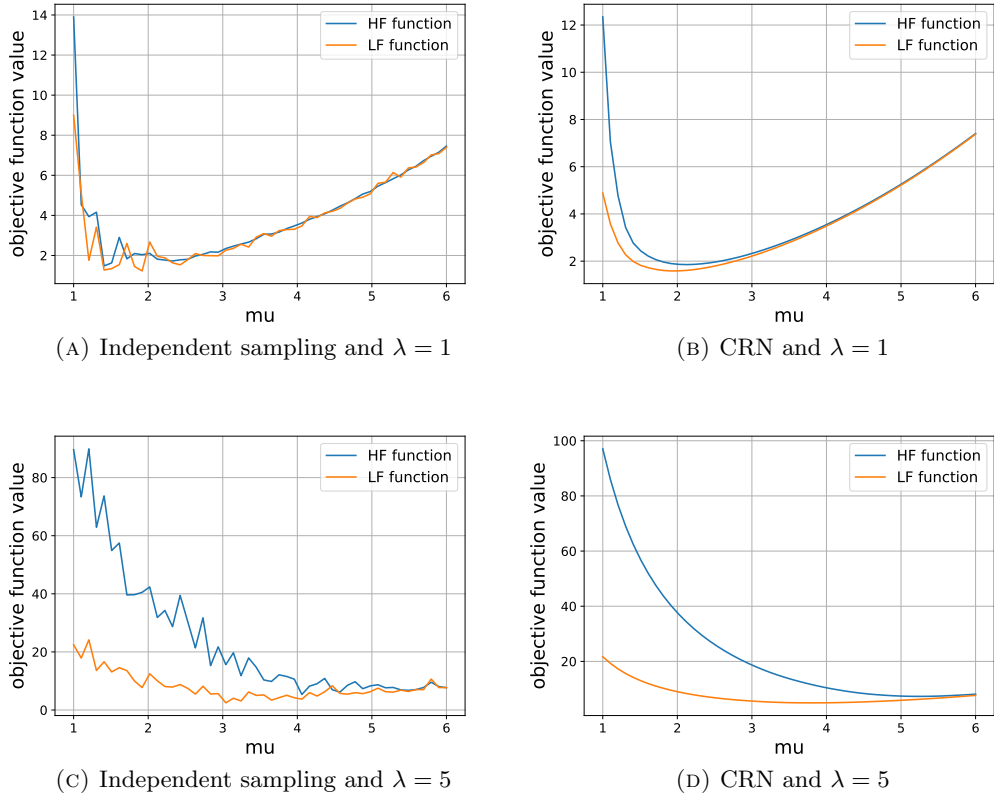


FIGURE 9: Objective function trajectories of the M/M/1 problem with and without CRN. When employing CRN, the LF and HF functions exhibit smoothness.

One important characteristic of the problem is that $F^h(\cdot, \xi)$ and $F^\ell(\cdot, \xi)$ are smooth functions for any $\xi^h \in \Xi^h$, as illustrated in Figure 9. The difficulty in addressing this problem with the LF function is that its gradient is relatively smaller compared to that of the HF function,

which becomes clearer when λ is large (see Figure 9c and 9d). In traditional TR methods, the criterion for successful iterations hinges on comparing the reduction in the model and the function estimates. Therefore, when the small gradient of the LF function leads to only a slight reduction in the model value, a candidate point can be accepted, albeit leading away from the optimal solution. To address this issue, the additional condition is introduced, $\tilde{F}_k(\mathbf{X}_k^0) - \tilde{F}_k(\mathbf{X}_k^{s,\ell}) \geq \eta\zeta(\Delta_k^h)^2$, for a successful iteration in Algorithm 3 (see Remark 2).

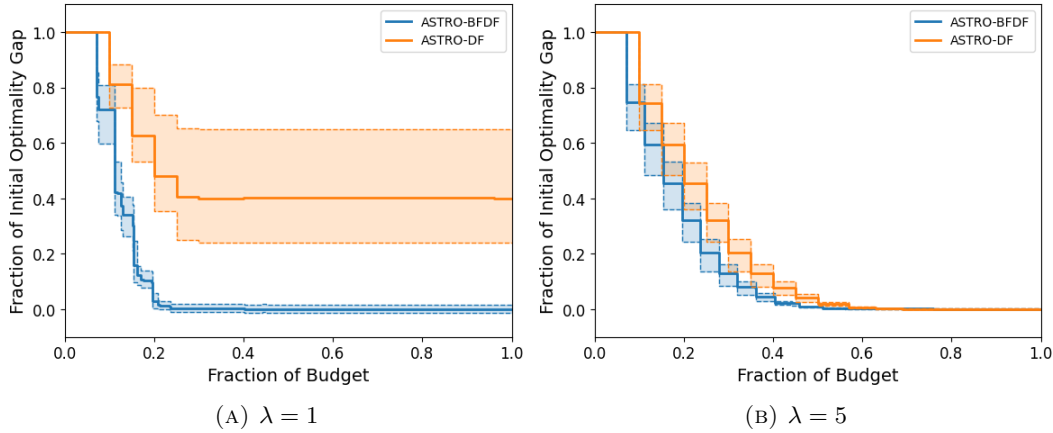


FIGURE 10: Fraction of the optimality gap with 95% confidence intervals from 20 runs of each algorithm.

We conducted experiments on 5 instances of the M/M/1 problem by varying λ across the range $\{1, 2, \dots, 5\}$, as shown in Figure 8. Figure 10 illustrates the optimization progress for two scenarios: one where $\lambda = 1$ and another where $\lambda = 5$. In the scenario where $\lambda = 1$, as the incumbents approach the optimal solution, it becomes essential for the TR to contract appropriately to achieve an accurate gradient approximation. While contracting the TR, ASTRO-DF exhausts its budget entirely, which explains its slower convergence in Figure 10a. In contrast, ASTRO-BFDF is capable of rapidly identifying a near-optimal solution. The primary reason is that the gradient of the LF-based local model is inherently small, enabling us to sustain successful iterations before the TR initiates sequential contraction. Conversely, when $\lambda = 5$, the gradient of the local model for the LF function becomes extremely small, prompting a termination of LF function utilization after just a few iterations. As a result, in Figure 10b, the optimization trajectory of ASTRO-BFDF appears similar to that of ASTRO-DF, but ASTRO-BFDF demonstrates slightly faster convergence due to the variance-reduced function estimates provided by BFAS.

5.2.2 (s, S) Inventory Problem

We now consider an (s, S) inventory model. At each time step t , the demand D_t , which follows an exponential distribution with mean μ_D , is generated. At the end of each time step, the inventory level is calculated as $I_t^e = I_t^s - D_t + O_t$, where I_t^e denotes the end-of-day inventory, I_t^s is the starting inventory on hand, and O_t is the amount of inventory that was ordered earlier and arrives on that day. If I_t^e is below s , an order is placed to restore the inventory up to S . Lead times follow a Poisson distribution with mean μ_L time steps. The objective is to find the best s and S for minimizing the average costs, which is composed of backorder costs, order costs, and holding costs. Backorder costs refer to penalties incurred when demand cannot be immediately

satisfied; order costs consist of a fixed cost applied whenever an order is placed, regardless of its size, and a variable cost based on the order quantity; and holding costs represent the cost of maintaining positive inventory at the end of each day. As in the M/M/1 problem, randomness in demands and lead times is captured by ξ^h ; thus, employing CRNs ensures that the same sequence of demands and lead times is used across different system configurations.

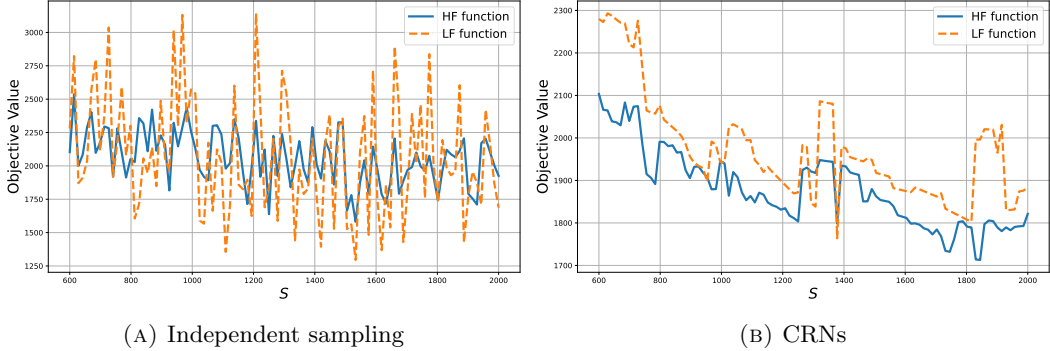


FIGURE 11: Objective function trajectories of the inventory problem with and without CRN, evaluated over varying S with fixed $s = 500$. The demand and lead time means are $\mu_D = 400$ and $\mu_L = 3$, respectively.

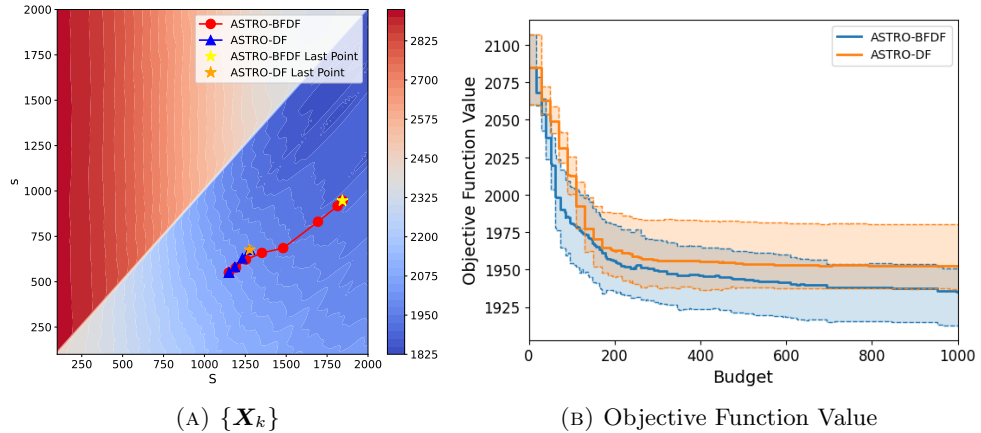


FIGURE 12: (a) illustrates a sample path of $\{X_k\}$ for ASTRO-DF and ASTRO-BFDF on the inventory problem with $\mu_D = 400$, $\mu_L = 3$, and a budget of 1000 HF evaluations, where contours represent objective function estimates based on 50 samples. (b) presents the average objective function value over 20 runs under the same setting.

This problem is significantly more challenging than the M/M/1 problem due to the inherent non-smoothness (see Figure 11). Therefore, it is highly probable that the majority of incumbent sequences converges to local optima, regardless of the solvers used. See Figure 12. Although ASTRO-BFDF may still converge to local optima (see Figure 13), it is generally more effective than ASTRO-DF at navigating the rugged objective landscape, often identifying better solutions by leveraging BF models. In particular, ASTRO-BFDF can explore a broader region of the search space by maintaining a larger Δ_k^h , increasing the likelihood of escaping poor local optima in practice. We tested 20 instances of the inventory problem with parameters combinations

$\mu_D = \{25, 50, 100, 200, 400\}$ and $\mu_L = \{1, 3, 6, 9\}$. In most cases, ASTRO-BFDF converged faster than ASTRO-DF, and sometimes achieved better solutions, as evidenced by its higher fraction of solved problems at the budget limit (see Figure 8).

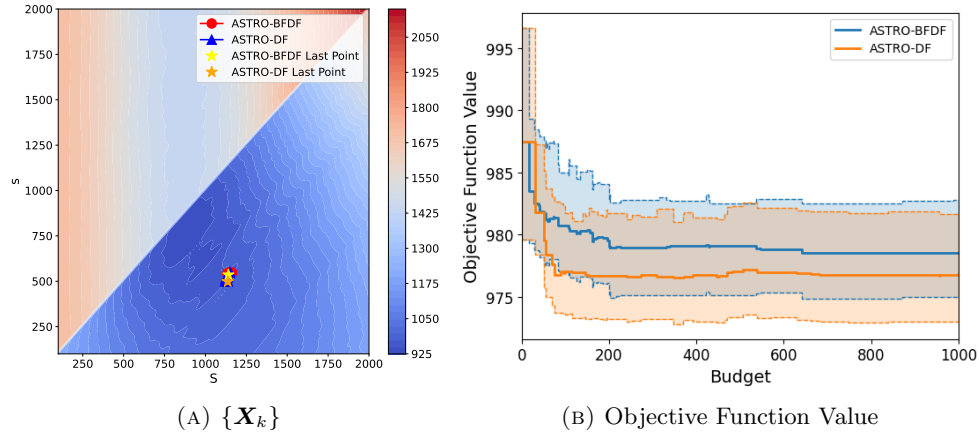


FIGURE 13: Same experimental setup as in Fig 12 but with different parameters with $\mu_D = 200$ and $\mu_L = 3$. Both ASTRO-DF and ASTRO-BFDF failed to escape convergence to poor solution and the average difference in objective values between the two solvers is less than 5.

6 Conclusion

This paper introduces ASTRO-BFDF, a novel stochastic TR algorithm tailored for addressing bi-fidelity simulation optimization. ASTRO-BFDF is characterized by two key features: First, it dynamically utilizes bi-fidelity Monte Carlo or crude Monte Carlo, adaptively adjusting sample sizes for both fidelity oracles within BFAS. Second, it guides incumbents toward the neighborhood of a stationary point of the HF function by utilizing the LF function. These two features enable faster convergence and improved computational efficiency, as demonstrated on synthetic and DES-based problems. We also demonstrate the asymptotic behavior of the incumbents generated by ASTRO-BFDF, which converges to the stationary point almost surely.

Acknowledgements

This work was authored by the National Renewable Energy Laboratory, operated by Alliance for Sustainable Energy, LLC, for the U.S. Department of Energy (DOE) under Contract No. DE-AC36-08GO28308. Funding for the algorithmic development and numerical experiment work was provided by Laboratory Directed Research and Development investments. The views expressed in the article do not necessarily represent the views of the DOE or the U.S. Government. The U.S. Government retains and the publisher, by accepting the article for publication, acknowledges that the U.S. Government retains a nonexclusive, paid-up, irrevocable, worldwide license to publish or reproduce the published form of this work, or allow others to do so, for U.S. Government purposes.

A Proof of Theorem 1

Proof. Let us first set $\bar{E}_k^{i,q}(N_k^i) = N(\mathbf{X}_k^i)^{-1} \sum_{j=1}^{N(\mathbf{X}_k^i)} E_{k,j}^{i,q}$ and $o_k = (\sigma_0^q)^2 \kappa^{-2} (\Delta_k^q)^{-4}$, implying $N(\mathbf{X}_k^i) \geq \lambda_k o_k$. Then we have

$$\begin{aligned} \mathbb{P} \left\{ |\bar{E}_k^{i,q}(N_k^i)| > c_f(\Delta_k^q)^2 \middle| \mathcal{F}_{k-1} \right\} &\leq \mathbb{P} \left\{ \sup_{n \geq \lambda_k o_k} |\bar{E}_k^{i,q}(n)| > c_f(\Delta_k^q)^2 \middle| \mathcal{F}_{k-1} \right\} \\ &\leq \sum_{n \geq \lambda_k o_k} \mathbb{P} \left\{ \left| \frac{1}{n} \sum_{j=1}^n E_{k,j}^{i,q} \right| > c_f(\Delta_k^q)^2 \middle| \mathcal{F}_{k-1} \right\} \\ &\leq \sum_{n \geq \lambda_k o_k} 2 \exp \left\{ \left(-n \frac{c_f^2(\Delta_k^q)^4}{(2c_f(\Delta_k^q)^2 b^q + 2(\sigma^q)^2)} \right) \right\} \\ &= \sum_{n \geq 0} 2 \exp(-c_k(\lambda_k o_k + n)) = 2 \frac{\exp(-\lambda_k c_k \nu_k)}{1 - \exp(-c_k)}, \end{aligned}$$

where $c_k = \frac{c_f^2(\Delta_k^q)^4}{2(c_f \Delta_{\max}^2 b^q + (\sigma^q)^2)}$. The third inequality is obtained using Assumption 2 and Lemma 1. Given that $\lambda_k = \lambda_0(\log k)^{1+\epsilon_\lambda}$ and $c_k o_k = \mathcal{O}(1)$, there exists some $\varepsilon > 0$ such that for sufficiently large k , the following holds.

$$\mathbb{P} \left\{ |\bar{E}_k^{i,q}(N_k^i)| \geq c_f(\Delta_k^q)^2 \right\} = \mathbb{E} \left[\mathbb{P} \left\{ |\bar{E}_k^{i,q}(N_k^i)| \geq c_f(\Delta_k^q)^2 \middle| \mathcal{F}_{k-1} \right\} \right] \leq k^{-1-\varepsilon}. \quad (32)$$

Since the right-hand side of (32) is summable in k , the theorem holds. \square

B Proof of Lemma 7

Proof. Let us begin by noting that we have established from Step 23 in Algorithm 2 and Step 9 in Algorithm 3 that $\Delta_k^h \geq \Delta_k^\ell$ almost surely for any $k \in \mathbb{N}$. Hence, if Δ_k^h converges to zero almost surely, so does Δ_k^ℓ . Let us define the following index sets,

$$\begin{aligned} \mathcal{H} &= \{k \in \mathbb{N} : (\hat{\rho}_k > \eta) \cap (\mu \|\nabla M_k^h(\mathbf{X}_k^0)\| \geq \Delta_k^h) \cap (I_k^h \text{ is True})\}, \\ \mathcal{L} &= \{k \in \mathbb{N} : I_k^h \text{ is False}\}. \end{aligned}$$

From Assumption 3, we have, for any $k \in \mathcal{H}$,

$$\begin{aligned} \tilde{F}(\mathbf{X}_k^0) - \tilde{F}(\mathbf{X}_k^s) &\geq \tilde{F}(\mathbf{X}_k^0) - \tilde{F}(\mathbf{X}_k^{s,h}) \geq \eta [M_k^h(\mathbf{X}_k^0) - M_k^h(\mathbf{X}_k^{s,h})] \\ &\geq \frac{1}{2} \eta \kappa_{fcd} \|\nabla M_k^h(\mathbf{X}_k^0)\| \min \left\{ \frac{\|\nabla M_k^h(\mathbf{X}_k^0)\|}{\|\mathbf{H}_k^h\|}, \Delta_k^h \right\} > \kappa_R (\Delta_k^h)^2, \end{aligned} \quad (33)$$

where $\kappa_R = \min\{\eta \kappa_{fcd} (2\mu)^{-1} \min\{(\mu \kappa_{\mathbf{H}}^h)^{-1}, 1\}, \zeta\}$. Note that (33) holds regardless of whether \mathbf{X}_k^s comes from minimizing M_k^ℓ or M_k^h . We also obtain from Step 6 in Algorithm 3 that, for any $k \in \mathcal{L}$,

$$\tilde{F}(\mathbf{X}_k^0) - \tilde{F}(\mathbf{X}_k^s) \geq \zeta (\Delta_k^h)^2 \geq \kappa_R (\Delta_k^h)^2. \quad (34)$$

Hence, for any $k \in \mathcal{K} = \mathcal{H} \cup \mathcal{L}$,

$$\kappa_R \sum_{k \in \mathcal{K}} (\Delta_k^h)^2 \leq \sum_{k \in \mathcal{K}} (f^h(\mathbf{X}_k) - f^h(\mathbf{X}_{k+1}) + \tilde{E}_k^0 - \tilde{E}_k^s) \leq f^h(\mathbf{x}_0) - f_*^h + \sum_{k=0}^{\infty} |\tilde{E}_k^0 - \tilde{E}_k^s|,$$

where f_*^h is the optimal value of f^h . We note that \mathcal{H} and \mathcal{L} are disjoint sets and for any $k \notin \mathcal{K}$, $\Delta_{k+1}^h = \gamma_2 \Delta_k^h$. Let $\mathcal{K} = \{k_1, k_2, \dots\}$, $k_0 = -1$, and $\Delta_{-1}^h = \Delta_0^h / \gamma_2$. Then from the fact that $\Delta_k^h \leq \gamma_1 \gamma_2^{k-k_i-1} \Delta_{k_i}^h$ for $k = k_i + 1, \dots, k_{i+1}$ and each i , we obtain

$$\sum_{k=k_i+1}^{k_{i+1}} (\Delta_k^h)^2 \leq \gamma_1^2 (\Delta_{k_i}^h)^2 \sum_{k=k_i+1}^{k_{i+1}} \gamma_2^{2(k-k_i-1)} \leq \gamma_1^2 (\Delta_{k_i}^h)^2 \sum_{k=0}^{\infty} \gamma_2^{2k} = \frac{\gamma_1^2}{1-\gamma_2^2} (\Delta_{k_i}^h)^2.$$

By Lemma 6 and the fact that $\Delta_k^\ell \leq \Delta_k^h$, there must exist a sufficiently large K_Δ such that $|\tilde{E}_k^0 - \tilde{E}_k^s| < c_\Delta (\Delta_k^h)^2$ for any given $c_\Delta > 0$ and any $k \geq K_\Delta$. Then, we have

$$\begin{aligned} \sum_{k=0}^{\infty} (\Delta_k^h)^2 &\leq \frac{\gamma_1^2}{1-\gamma_2^2} \sum_{i=0}^{\infty} (\Delta_{k_i}^h)^2 < \frac{\gamma_1^2}{1-\gamma_2^2} \left(\frac{(\Delta_0^h)^2}{\gamma_2^2} + \frac{f^h(\mathbf{x}_0) - f_*^h + E'_{0,\infty}}{\kappa_R} \right) \\ &< \frac{\gamma_1^2}{1-\gamma_2^2} \left(\frac{(\Delta_0^h)^2}{\gamma_2^2} + \frac{f^h(\mathbf{x}_0) - f_*^h + E'_{0,K_\Delta-1} + E'_{K_\Delta,\infty}}{\kappa_R} \right), \end{aligned}$$

where $E'_{i,j} = \sum_{k=i}^j |\tilde{E}_k^0 - \tilde{E}_k^s|$. Then we get from $E'_{K_\Delta,\infty} < c_\Delta \sum_{K_\Delta}^{\infty} (\Delta_k^h)^2$ that

$$\sum_{k=K_\Delta}^{\infty} (\Delta_k^h)^2 < \frac{\gamma_1^2}{1-\gamma_2^2} \left(\frac{(\Delta_0^h)^2}{\gamma_2^2} + \frac{f^h(\mathbf{x}_0) - f_*^h + E'_{0,K_\Delta-1}}{\kappa_R} \right) \left(1 - \frac{\gamma_1^2}{1-\gamma_2^2} \frac{c_\Delta}{\kappa_R} \right)^{-1}$$

Therefore, $\Delta_k^h \xrightarrow{w.p.1} 0$ as $k \rightarrow \infty$ and the statement of the theorem holds. \square

C Proof of Theorem 9

The proof trivially follows from Lemma 4.4 with the adaptive sampling rule (A-0) in [35].

Proof. Let $\omega \in \Omega$ and we will omit ω to simplify notation. We first note that for any $k \in \mathbb{N}$, when the minimizer of the LF-based local model in Algorithm 3 is accepted as a next iterate, I_k^h is already False. Otherwise, the HF-based local model is constructed in Algorithm 2. Then we have

$$M_k^h(\mathbf{X}_k^{s,h}) = \tilde{F}(\mathbf{X}_k^0) + \nabla M_k^h(\mathbf{X}_k^0)^\top \mathbf{S}_k + \frac{1}{2} \mathbf{S}_k^\top \mathbf{H}_k^h \mathbf{S}_k, \quad (35)$$

where \mathbf{S}_k is the step size. We also know from Taylor's theorem that

$$\tilde{F}(\mathbf{X}_k^{s,h}) = f^h(\mathbf{X}_k^0) + \nabla f^h(\mathbf{X}_k^0)^\top \mathbf{S}_k + \int_0^1 \left(\nabla f^h(\mathbf{X}_k^0 + t\mathbf{S}_k) - \nabla f^h(\mathbf{X}_k^0) \right)^\top \mathbf{S}_k dt + \tilde{E}_k^s. \quad (36)$$

By subtracting (35) by (36), we can obtain, for sufficiently large k ,

$$\begin{aligned} |M_k^h(\mathbf{X}_k^{s,h}) - \tilde{F}(\mathbf{X}_k^{s,h})| &\leq |(\nabla M_k^h(\mathbf{X}_k^0) - \nabla f^h(\mathbf{X}_k^0))^\top \mathbf{S}_k| + \frac{1}{2} \left| \mathbf{S}_k^\top \mathbf{H}_k^h \mathbf{S}_k \right| + |\tilde{E}_k^0 - \tilde{E}_k^s| \\ &\quad + \left| \int_0^1 (\nabla f(\mathbf{X}_k^0 + t\mathbf{S}_k) - \nabla f(\mathbf{X}_k^0))^\top \mathbf{S}_k dt \right| \\ &\leq (\kappa_{eg1} + 2p\kappa_{eg2}c_f)(\Delta_k^h)^2 + 2c_f(\Delta_k^h)^2 + \frac{1}{2}(\kappa_{Lg} + \kappa_{\mathbf{H}}^h)(\Delta_k^h)^2, \end{aligned} \quad (37)$$

where the last inequality follows from (21), Lemma 6, and Assumptions 1 and 4. Moreover, we have from Assumption 3 and $\Delta_k^h \leq c_d \|\nabla M_k^h(\mathbf{X}_k^0)\|$ that

$$\begin{aligned} M_k^h(\mathbf{X}_k^0) - M_k^h(\mathbf{X}_k^{s,h}) &\geq \frac{1}{2} \kappa_{fcd} \|\nabla M_k^h(\mathbf{X}_k^0)\| \min \left\{ \frac{\|\nabla M_k^h(\mathbf{X}_k^0)\|}{\|\nabla^2 M_k^h(\mathbf{X}_k^0)\|}, \Delta_k^h \right\} \\ &\geq \frac{1}{2c_d} \kappa_{fcd} \min \left\{ \frac{1}{c_d \kappa_{\mathbf{H}}^h}, 1 \right\} (\Delta_k^h)^2 \end{aligned} \quad (38)$$

Then we obtain from (37) and (38) that the success ratio becomes

$$|1 - \hat{\rho}_k| = \frac{|M_k^h(\mathbf{X}_k^{s,h}) - \tilde{F}(\mathbf{X}_k^{s,h})|}{|M_k^h(\mathbf{X}_k^0) - M_k^h(\mathbf{X}_k^{s,h})|} \leq \frac{(\kappa_{eg1} + 2p\kappa_{eg2}c_f + 2c_f + \frac{1}{2}(\kappa_{Lg} + \kappa_{\mathbf{H}}^h))(\Delta_k^h)^2}{(2c_d)^{-1} \kappa_{fcd} \min\{(c_d \kappa_{\mathbf{H}}^h)^{-1}, 1\} (\Delta_k^h)^2}.$$

As a result, when $c_d \leq ((1 - \eta)\kappa_{cf})((2\kappa_{eg1} + 4p\kappa_{eg2}c_f + 4c_f + \kappa_{Lg} + \kappa_{\mathbf{H}}^h)^{-1}$, we have $\hat{\rho}_k \geq \eta$, proving the sought result. \square

D Implementation Details

The two most important hyperparameters are the step sizes and sample sizes for the solvers. To tune them, we tested a range of values for each solver on synthetic problems with the cost ratio 1 : 0.1 and problems with DES. In this section, we present the detailed setup for the optimizers used in Section 5, including the hyperparameter tuning of sample sizes and step sizes. We begin with ASTRO-DF and ASTRO-BFDF.

D.1 Setup for ASTRO-DF and ASTRO-BFDF

ASTRO-DF and ASTRO-MFDF used the same parameters (e.g., TR radius Δ_k , success ratio η_1) where possible. In terms of the design set selection for the model construction, ASTRO-DF has used $2d + 1$ design points with the rotated coordinate basis (See history-informed ASTRO-DF [46]). In the bi-fidelity scenario, we have employed two distinct design sets (\mathcal{X}_k and \mathcal{X}_k^ℓ) at Step 14 in Algorithm 2 and Step 1 in Algorithm 3 respectively. \mathcal{X}_k is selected to construct the local model for the HF function, implying that the computational costs for estimating the function value at \mathcal{X}_k is relatively high. Hence, the design set will be selected by reusing the design points within the TR and the corresponding replications as much as possible. To achieve this, we first pick $d + 1$ design points to obtain sufficiently affinely independent points by employing Algorithm 4.2 in [47]. After that, we pick additional d design points following the opposite direction to construct the quadratic interpolation model with diagonal Hessian. \mathcal{X}_k^ℓ consists of $2d + 1$ design points, selected using the coordinate basis to minimize deterministic error owing to the lower cost of the LF oracle. In this scenario, the design set \mathcal{X}_k^ℓ is optimally designed for design sets of any size ranging from $d + 2$ to $2d + 1$ (see [48]).

For hyperparameter tuning, since the sample size and step size controlled by trust-region radius, we focused on the initial trust-region radius, which is the primary hyperparameter affecting performance. When box constraints exist, it is natural to set the initial trust region as a portion of the feasible region. Since all synthetic problems have box constraints, we set Δ_0^h and Δ_k^ℓ to $c_\Delta \times 0.1 \times \min_{i \in 1, 2, \dots, d} (u_i - l_i)$, where c_Δ is a positive constant, and u_i and l_i denote the upper and lower bounds for the i -th coordinate, respectively. We first tested $c_\Delta \in \{0.5, 1, 1.5, 2\}$ on synthetic problems. See Figure 14a and 14b. In contrast, DES-based problems do not have box constraints. Instead, each problem can generate random solutions based on the input parameters provided by

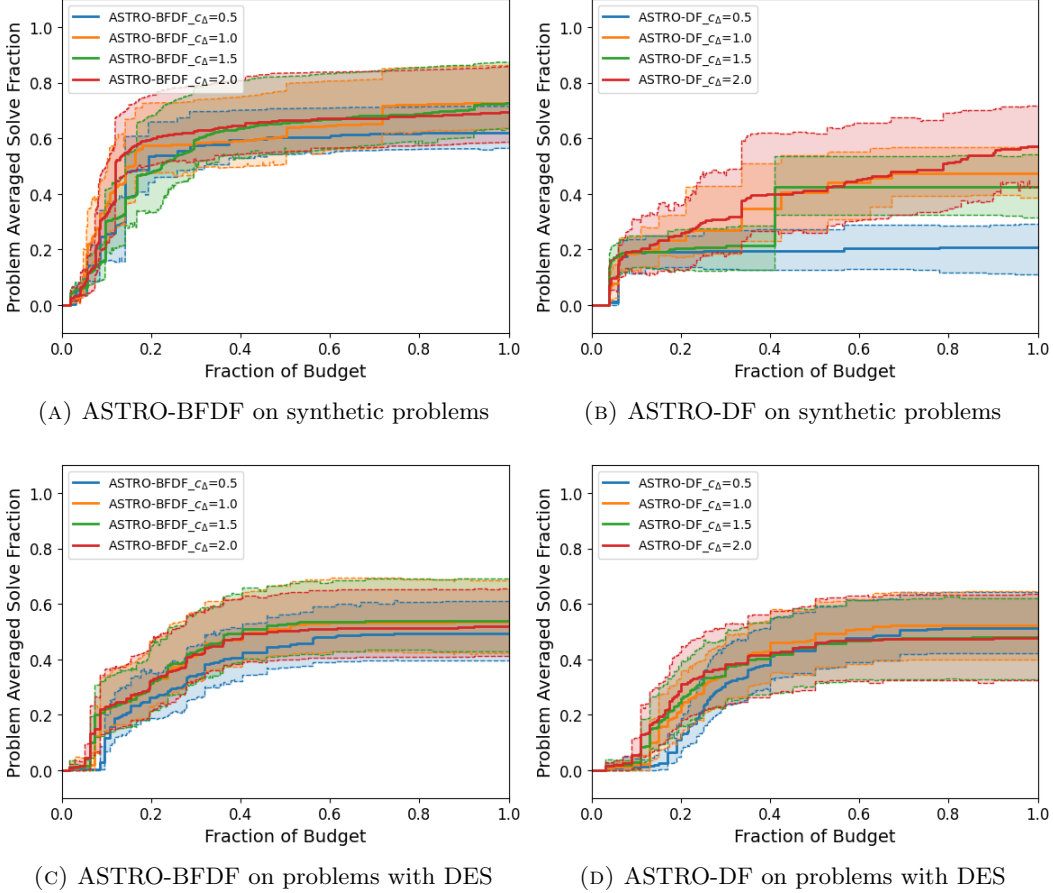


FIGURE 14: Solvability profiles with 1% optimality gap for hyperparameter tuning of ASTRO-BFDF and ASTRO-DF.

SimOpt [49]. Accordingly, we generated $1000 \times d$ random solutions $\{\mathbf{X}^r\}$, where r indexes each of the $1000 \times d$ solutions, and set Δ_0^h and Δ_0^ℓ to $c_\Delta \sum_{i=1}^d (\max_r \{X_i^r\} - \min_r \{X_i^r\})$, where X_i^r denoted the i -th coordinate of \mathbf{X}^r . We tested $c_\Delta \in \{0.5, 1.0, 1.5, 2\}$ on DES-based problems as well. See Figure 14c and 14d. As a result, we use $c_\Delta = 2$ for ASTRO-BFDF and ASTRO-DF in Section 5.

D.2 Setup for ADAM and BFSAG

Since ADAM and BFSAG are designed for settings where gradient information is directly available, we approximate the gradient for the targeted problem (1) using the finite-difference method, with the perturbation constant set equal to the step size. The sample sizes n is used to estimate the function value and the gradient is approximated using the function estimates. In BFSAG, the sample size for high-fidelity simulations is set to n , while the sample size for low-fidelity simulations is set to $2n$. For hyper-parameter tuning, we first fix n as 10 and tested variety step sizes from 0.01 to 2 (Figure 16a and 16c). After that, we chose the best step sizes for each solver and tested various $n \in \{10, 20, 30\}$ (Figure 16b and 16d). As a result, $lr = 1$ and $n = 10$ for ADAM and $lr = 0.01$ and $n = 10$ for BFSAG is used in the synthetic problems presented in Section 5.

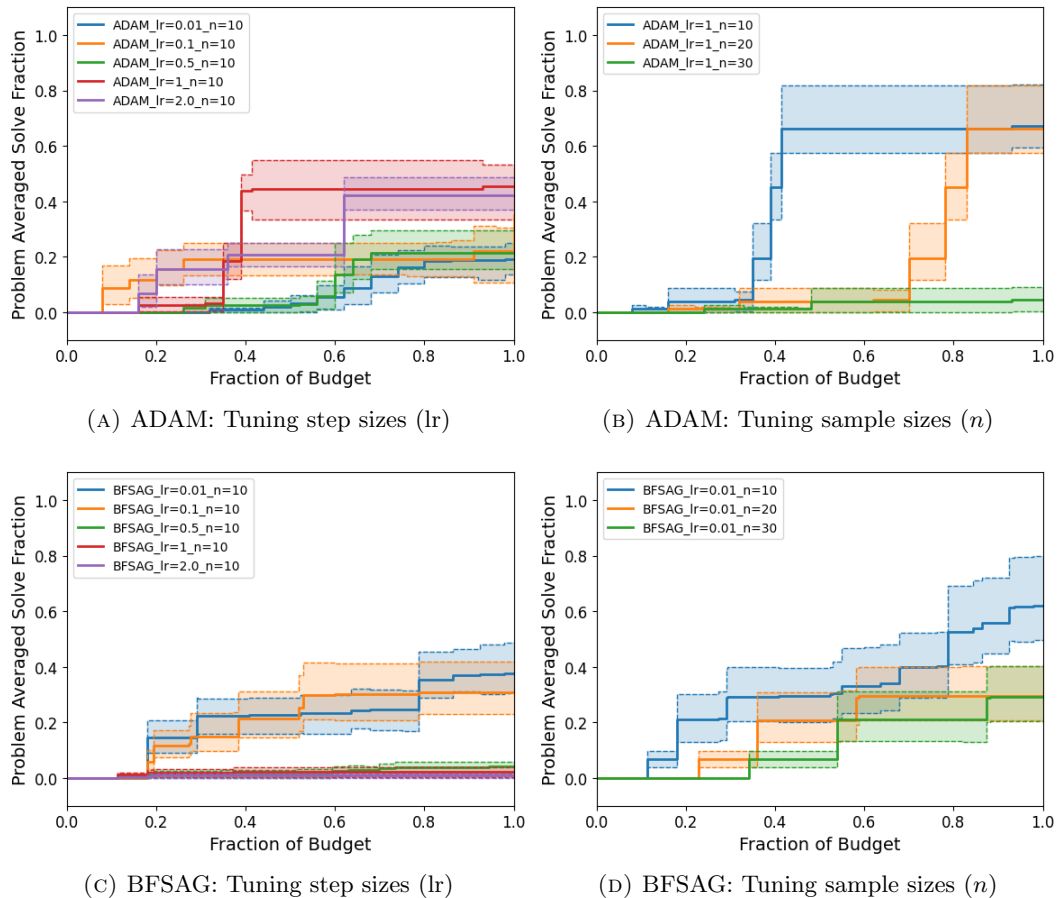


FIGURE 15: Solvability profiles for hyperparameter tuning of ADAM and BFSAG on synthetic problems. (a) and (c) show the impact of different step sizes with a fixed sample size ($n = 10$), while (b) and (d) show the impact of different sample sizes with the best step size found in (a) and (c).

For the DES-based problems, we again tuned the step sizes first with $n = 10$, and then tuned the sample sizes. We used the same step size setup as ASTRO-BFDF to ensure a fair comparison, i.e., $lr = c_\Delta \sum_{i=1}^d (\max_r \{X_i^r\} - \min_r \{X_i^r\})$, where X_i^r denoted the i -th coordinate of \mathbf{X}^r . We tested $c_\Delta \in \{0.5, 1.0, 1.5, 2\}$ and $n \in \{10, 20, 30\}$ on DES-based problems as well. See Figure 14c. As result, we use $c_\Delta = 2$ and $n = 10$ for ADAM and BFSAG on the DES-based problems in

Section 5.

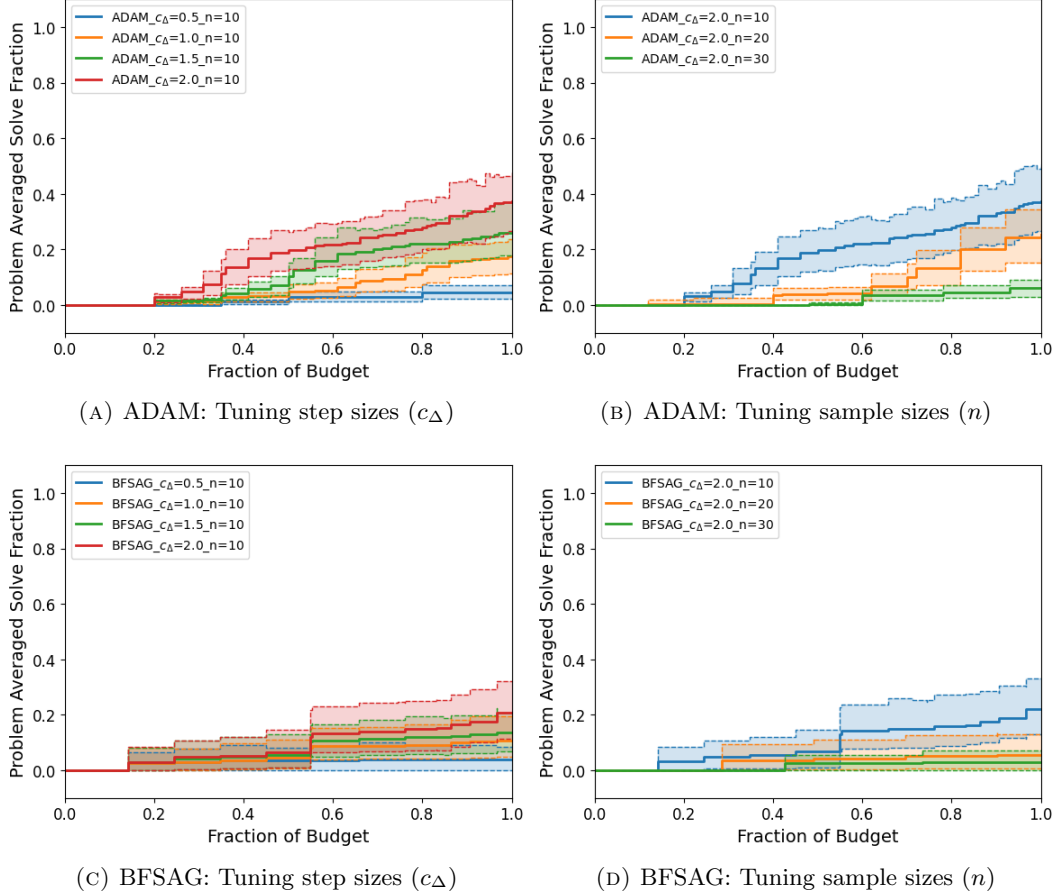


FIGURE 16: Solvability profiles for hyperparameter tuning of ADAM and BFSAG on problems with DES. (a) and (c) show the impact of different step sizes with a fixed sample size ($n = 10$), while (b) and (d) show the impact of different sample sizes with the best step size found in (a) and (c).

D.3 Setup for BFBO

Since BFBO is a global optimizer, a step size is not required. Instead, the next candidate is selected by optimizing an acquisition function. Expected improvement combined with stochastic co-kriging is used as the acquisition function, following the widely adopted standard for bi-fidelity Bayesian optimization discussed in Section 1. The stochastic co-kriging model is implemented using SMT [50] in Section 5. With the similar setup with BFSAG, the sample size for high-fidelity simulations is set to n , while the sample size for low-fidelity simulations is set to $2n$. In particular, when the new design points are selected by minimizing the expected improvement, the HF and LF function estimates are obtained by (2) with n and $2n$ replications, respectively. The co-kriging model is then retrained using all available function estimates. For hyper-parameter tuning, we tested $n \in \{10, 20, 30\}$. See Figure 17. While $n = 10$ provides the best setup, generating a single sample path of $\{\mathbf{X}_k\}$ can take over an hour for the 20-dimensional stochastic Rosenbrock function with a budget of 4,000 high-fidelity evaluations, due to the need to retrain the co-kriging model each time a new design point is explored. For reference, generating a sample path using ASTRO-MFDF typically takes less than five minutes with the same setup.

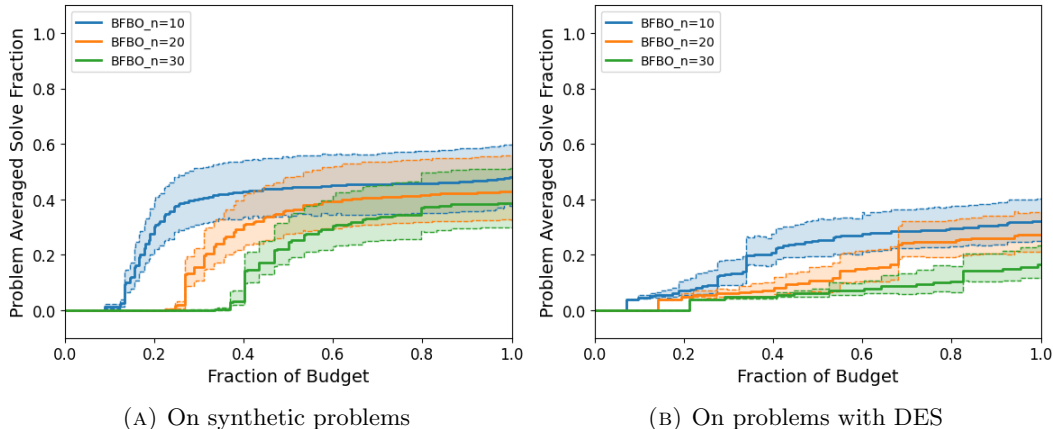


FIGURE 17: Solvability profiles with 1% optimality gap for hyperparameter tuning of BFBO.

E Bi-fidelity Deterministic Functions

This section provides details on the bi-fidelity deterministic functions used in Section 5. Four deterministic HF functions are used in total: three benchmark problems—Branin, Colville, and Forrester functions—are taken from [40], while the fourth, the Rosenbrock function, is adapted for bi-fidelity optimization as introduced in [51]. We begin by presenting the closed-form expressions of the functions and the corresponding problem dimensions (see Table 1). Since Branin, Colville, and Rosenbrock are multi-dimensional functions, all variables are fixed except $x[1]$, which is varied to visualize the loss landscape and provide intuition about the effect of κ_{cor} (See Figure 18, 19, and 20). The loss landscapes for the Forrester functions are shown in Figure 2. Overall, as κ_{cor} increases, the LF function f^l appears to provide more useful information for optimizing the HF function f^h .

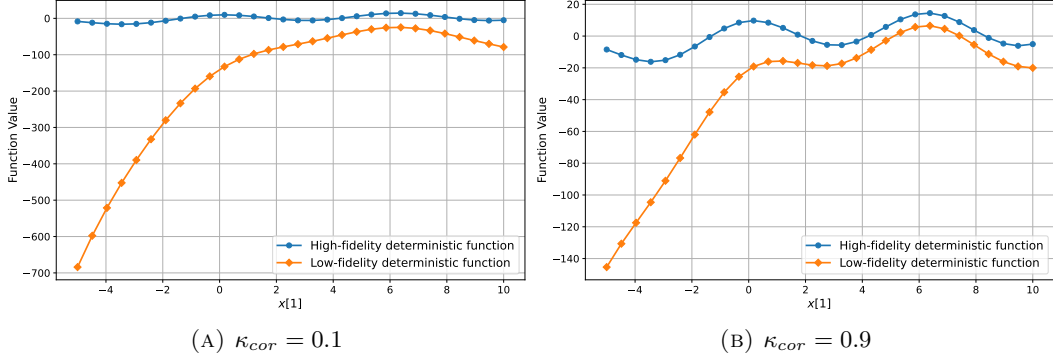


FIGURE 18: Marginalized loss landscapes of the Branin function with two different κ_{cor} values, obtained by varying $x[1]$ while keeping all other elements fixed.

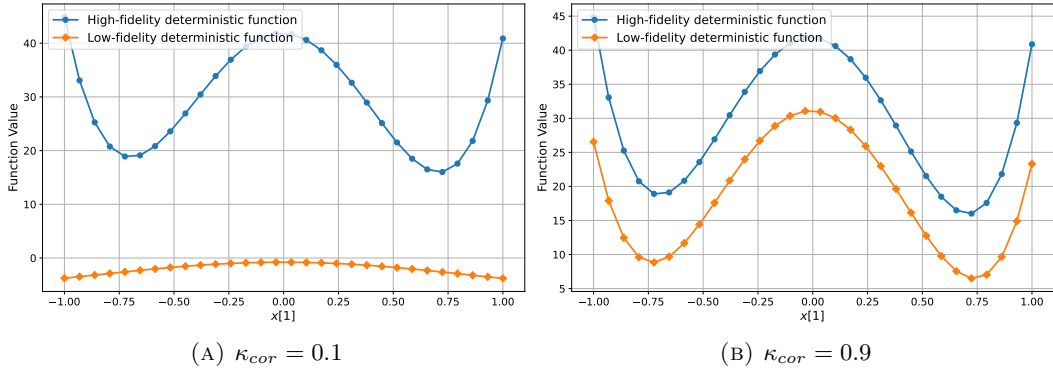


FIGURE 19: Marginalized loss landscapes of the Colville function with two different κ_{cor} values, obtained by varying $x[1]$ while keeping all other elements fixed.

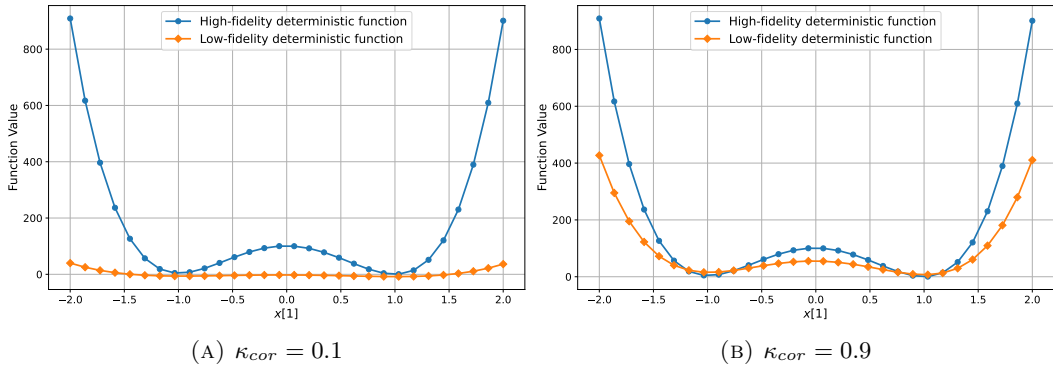


FIGURE 20: Marginalized loss landscapes of the Rosenbrock function with two different κ_{cor} values, obtained by varying $x[1]$ while keeping all other elements fixed.

Function	Equation(s)	Dimension
Forretal	$\cdot f^h(\mathbf{x}) = (6x - 2)^2 \sin(12x - 4)$ $\cdot f^\ell(\mathbf{x}) = (-2 - \kappa_{cor}^2 + 4\kappa_{cor})f^h + 10(x - 0.5) - 5$	1
Branin	$\cdot f^h(\mathbf{x}) = (x[2] - \frac{5.1}{4\pi^2}x[1]^2 + \frac{5}{\pi}x[1] - 6)^2$ $+ 10\left(1 - \frac{1}{8\pi}\right) \cos x[1] + 10$ $\cdot f^\ell(\mathbf{x}) = f^h - (0.5\kappa_{cor}^2 - 2\kappa_{cor} + 1.7)$ $\cdot (x[2] - \frac{5.1}{4\pi^2}x[1]^2 + \frac{5}{\pi}x[1] - 6)^2$	2
Colville	$\cdot f^h(\mathbf{x}) = 100(x[1]^2 - x[2])^2 + (x[1] - 1)^2 + (x[3] - 1)^2$ $+ 10.1((x[2] - 1)^2 + (x[4] - 1)^2)$ $+ 19.8(x[2] - 1)(x[4] - 1) + 90(x[3]^2 - x[4])^2$ $\cdot f^\ell(\mathbf{x}) = f^h(\kappa_{cor}^2 \mathbf{x})$ $-(\kappa_{cor} + 0.5)(5x[1]^2 + 4x[2]^2 + 3x[3]^2 + x[4]^2)$	4
Rosenbrock	$\cdot f^h(\mathbf{x}) = \sum_{i=1}^{D-1} [100(x[i+1] - x[i])^2 + (1 - x[i])^2]$ $\cdot f^\ell(\mathbf{x}) = \kappa_{cor} \sum_{i=1}^{D-1} [50(x[i+1] - x[i])^2 + (-2 - x[i])^2]$ $- \sum_{i=1}^D 0.5x[i]$	20

TABLE 1: Bi-fidelity deterministic functions

References

- [1] L. Y. Hsieh, E. Huang, and C.-H. Chen, “Equipment utilization enhancement in photolithography area through a dynamic system control using multi-fidelity simulation optimization with big data technique,” *IEEE Transactions on Semiconductor Manufacturing*, vol. 30, no. 2, pp. 166–175, 2017.
- [2] Y. Kang, L. Mathesen, G. Pedrielli, F. Ju, and L. H. Lee, “Multifidelity modeling for analysis and optimization of serial production lines,” *IEEE Transactions on Automatic Control*, vol. 66, no. 8, pp. 3460–3474, 2020.
- [3] Z. Zhang, Z. Guan, Y. Gong, D. Luo, and L. Yue, “Improved multi-fidelity simulation-based optimisation: application in a digital twin shop floor,” *International Journal of Production Research*, vol. 60, no. 3, pp. 1016–1035, 2022.
- [4] A. Chaudhuri, J. Jasa, J. R. Martins, and K. E. Willcox, “Multifidelity optimization under uncertainty for a tailless aircraft,” in *2018 AIAA Non-Deterministic Approaches Conference*, p. 1658, 2018.
- [5] K. M. Hamdia, H. Ghasemi, X. Zhuang, and T. Rabczuk, “Multilevel monte carlo method for topology optimization of flexoelectric composites with uncertain material properties,” *Engineering Analysis with Boundary Elements*, vol. 134, pp. 412–418, 2022.
- [6] M. Pisaroni, “Multi level monte carlo methods for uncertainty quantification and robust design optimization in aerodynamics,” tech. rep., EPFL, 2017.
- [7] M. Pisaroni, F. Nobile, and P. Leyland, “A continuation multi level monte carlo (c-mlmc) method for uncertainty quantification in compressible inviscid aerodynamics,” *Computer Methods in Applied Mechanics and Engineering*, vol. 326, pp. 20–50, 2017.
- [8] X. Chen, S. Hemmati, and F. Yang, “Stochastic co-kriging for steady-state simulation metamodeling,” in *2017 Winter Simulation Conference (WSC)*, pp. 1750–1761, IEEE, 2017.
- [9] B. Do and R. Zhang, “Multi-fidelity bayesian optimization: A review,” *arXiv preprint arXiv:2311.13050*, 2024.
- [10] R. Charayron, T. Lefebvre, N. Bartoli, and J. Morlier, “Towards a multi-fidelity & multi-objective bayesian optimization efficient algorithm,” *Aerospace Science and Technology*, vol. 142, p. 108673, 2023.
- [11] M. Meliani, N. Bartoli, T. Lefebvre, M.-A. Bouhlel, J. R. Martins, and J. Morlier, “Multi-fidelity

efficient global optimization: Methodology and application to airfoil shape design,” in *AIAA aviation 2019 forum*, p. 3236, 2019.

[12] L. Shu, P. Jiang, and Y. Wang, “A multi-fidelity bayesian optimization approach based on the expected further improvement,” *Structural and Multidisciplinary Optimization*, vol. 63, no. 4, pp. 1709–1719, 2021.

[13] A. Tran, T. Wildey, and S. McCann, “sbf-bo-2cogp: A sequential bi-fidelity constrained bayesian optimization for design applications,” in *International Design Engineering Technical Conferences and Computers and Information in Engineering Conference*, vol. 59179, p. V001T02A073, American Society of Mechanical Engineers, 2019.

[14] K. Xu, L. Shu, L. Zhong, P. Jiang, and Q. Zhou, “A bi-fidelity bayesian optimization method for multi-objective optimization with a novel acquisition function,” *Structural and Multidisciplinary Optimization*, vol. 66, no. 3, p. 53, 2023.

[15] S. Daulton, M. Balandat, and E. Bakshy, “Parallel bayesian optimization of multiple noisy objectives with expected hypervolume improvement,” *Advances in Neural Information Processing Systems*, vol. 34, pp. 2187–2200, 2021.

[16] B. Letham, B. Karrer, G. Ottoni, and E. Bakshy, “Constrained bayesian optimization with noisy experiments,” *Bayesian Analysis*, 2019.

[17] V. Picheny and D. Ginsbourger, “Noisy kriging-based optimization methods: a unified implementation within the diceoptim package,” *Computational Statistics & Data Analysis*, vol. 71, pp. 1035–1053, 2014.

[18] S. Diwale, M. K. Eisner, C. Carpenter, W. Sun, G. C. Rutledge, and R. D. Braatz, “Bayesian optimization for material discovery processes with noise,” *Molecular Systems Design & Engineering*, vol. 7, no. 6, pp. 622–636, 2022.

[19] Z. Z. Foumani, A. Yousefpour, M. Shishehbor, and R. Bostanabad, “On the effects of heterogeneous errors on multi-fidelity bayesian optimization,” *arXiv preprint arXiv:2309.02771*, 2023.

[20] N. Andrés-Thió, M. A. Muñoz, and K. Smith-Miles, “Characterising harmful data sources when constructing multi-fidelity surrogate models,” *arXiv preprint arXiv:2403.08118*, 2024.

[21] D. J. Toal, “Some considerations regarding the use of multi-fidelity kriging in the construction of surrogate models,” *Structural and Multidisciplinary Optimization*, vol. 51, pp. 1223–1245, 2015.

[22] R. Bollapragada, R. Byrd, and J. Nocedal, “Adaptive sampling strategies for stochastic optimization,” *SIAM Journal on Optimization*, vol. 28, no. 4, pp. 3312–3343, 2018.

[23] R. Bollapragada and S. M. Wild, “Adaptive sampling quasi-newton methods for zeroth-order stochastic optimization,” *Mathematical Programming Computation*, vol. 15, no. 2, pp. 327–364, 2023.

[24] S. Shashaani, F. S. Hashemi, and R. Pasupathy, “ASTRO-DF: A class of adaptive sampling trust-region algorithms for derivative-free stochastic optimization,” *SIAM Journal on Optimization*, vol. 28, no. 4, pp. 3145–3176, 2018.

[25] R. Bollapragada, C. Karamanli, and S. M. Wild, “Derivative-free optimization via adaptive sampling strategies,” *arXiv preprint arXiv:2404.11893*, 2024.

[26] B. Peherstorfer, K. Willcox, and M. Gunzburger, “Optimal model management for multifidelity monte carlo estimation,” *SIAM Journal on Scientific Computing*, vol. 38, no. 5, pp. A3163–A3194, 2016.

[27] B. Peherstorfer, P. S. Beran, and K. E. Willcox, “Multifidelity monte carlo estimation for large-scale uncertainty propagation,” in *2018 AIAA Non-Deterministic Approaches Conference*, p. 1660, 2018.

[28] Y. Yao, X. Huan, and J. Capecelatro, “Multi-fidelity uncertainty quantification of particle deposition in turbulent pipe flow,” *Journal of Aerosol Science*, vol. 166, p. 106065, 2022.

[29] J. Blanchet, C. Cartis, M. Menickelly, and K. Scheinberg, “Convergence rate analysis of a stochastic trust-region method via supermartingales,” *INFORMS journal on optimization*, vol. 1, no. 2, pp. 92–119, 2019.

[30] K.-H. Chang, L. J. Hong, and H. Wan, “Stochastic trust-region response-surface method (strong)—a new response-surface framework for simulation optimization,” *INFORMS Journal on Computing*, vol. 25, no. 2, pp. 230–243, 2013.

- [31] R. Chen, M. Menickelly, and K. Scheinberg, “Stochastic optimization using a trust-region method and random models,” *Mathematical Programming*, vol. 169, no. 2, pp. 447–487, 2018.
- [32] F. E. Curtis and Q. Wang, “Worst-case complexity of trace with inexact subproblem solutions for nonconvex smooth optimization,” *SIAM Journal on Optimization*, vol. 33, no. 3, pp. 2191–2221, 2023.
- [33] A. R. Conn, K. Scheinberg, and L. N. Vicente, *Introduction to derivative-free optimization*. Society for Industrial and Applied Mathematics, 1st ed., 2009.
- [34] P. Billingsley, *Probability and Measure*. Wiley Series in Probability and Mathematical Statistics, New York: John Wiley & Sons, 3rd ed., 1995.
- [35] Y. Ha, S. Shashaani, and R. Pasupathy, “Complexity of zeroth-and first-order stochastic trust-region algorithms,” *arXiv preprint arXiv:2405.20116*, 2024.
- [36] M. Ghosh, N. Mukhopadhyay, and P. K. Sen, *Sequential Estimation*. Wiley Series in Probability and Statistics, Wiley, 1 ed., 1997.
- [37] D. Williams, *Probability with martingales*. Cambridge university press, 1991.
- [38] L. Lv, C. Zong, C. Zhang, X. Song, and W. Sun, “Multi-fidelity surrogate model based on canonical correlation analysis and least squares,” *Journal of Mechanical Design*, vol. 143, no. 2, p. 021705, 2021.
- [39] J. Müller, “An algorithmic framework for the optimization of computationally expensive bi-fidelity black-box problems,” *INFOR: Information Systems and Operational Research*, vol. 58, no. 2, pp. 264–289, 2020.
- [40] X. Song, L. Lv, W. Sun, and J. Zhang, “A radial basis function-based multi-fidelity surrogate model: exploring correlation between high-fidelity and low-fidelity models,” *Structural and Multidisciplinary Optimization*, vol. 60, pp. 965–981, 2019.
- [41] Y. Ha and S. Shashaani, “Iteration complexity and finite-time efficiency of adaptive sampling trust-region methods for stochastic derivative-free optimization,” *arXiv:2305.10650*, 2023.
- [42] A. R. Conn, N. I. M. Gould, and P. L. Toint, *Trust Region Methods*. Society for Industrial and Applied Mathematics.
- [43] D. J. Eckman, S. G. Henderson, and S. Shashaani, “Diagnostic tools for evaluating and comparing simulation-optimization algorithms,” *INFORMS Journal on Computing*, vol. 35, no. 2, pp. 350–367, 2023.
- [44] S. De, K. Maute, and A. Doostan, “Bi-fidelity stochastic gradient descent for structural optimization under uncertainty,” *Computational Mechanics*, vol. 66, pp. 745–771, 2020.
- [45] D. P. Kingma and J. Ba, “Adam: A method for stochastic optimization,” 2017.
- [46] Y. Ha and S. Shashaani, “Towards greener stochastic derivative-free optimization with trust regions and adaptive sampling,” in *2023 Winter Simulation Conference (WSC)*, pp. 3508–3519, IEEE, 2023.
- [47] S. M. Wild, R. G. Regis, and C. A. Shoemaker, “Orbit: Optimization by radial basis function interpolation in trust-regions,” *SIAM Journal on Scientific Computing*, vol. 30, no. 6, pp. 3197–3219, 2008.
- [48] T. M. Ragonneau and Z. Zhang, “An optimal interpolation set for model-based derivative-free optimization methods,” *arXiv preprint arXiv:2302.09992*, 2023.
- [49] D. J. Eckman, S. G. Henderson, S. Shashaani, and R. Pasupathy, “SimOpt.” <https://github.com/simopt-admin/simopt>, 2023.
- [50] P. Saves, R. Lafage, N. Bartoli, Y. Diouane, J. Bussemaker, T. Lefebvre, J. T. Hwang, J. Morlier, and J. R. R. A. Martins, “SMT 2.0: A surrogate modeling toolbox with a focus on hierarchical and mixed variables gaussian processes,” *Advances in Engineering Software*, vol. 188, p. 103571, 2024.
- [51] L. Mainini, A. Serani, M. P. Rumpfkeil, E. Minisci, D. Quagliarella, H. Pehlivan, S. Yildiz, S. Ficini, R. Pellegrini, F. Di Fiore, *et al.*, “Analytical benchmark problems for multifidelity optimization methods,” *arXiv preprint arXiv:2204.07867*, 2022.